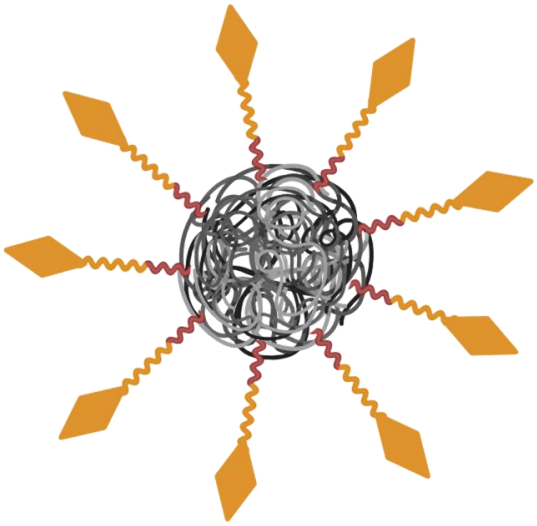
Biological evaluation of bioengineered precision antimicrobial nanoparticles for gastric infection

Clara Pinto Bessa
Master in Biochemistry,
Department of Chemistry and Biochemistry,
Faculty of Sciences of the University of Porto and School of Medicine and Biomedical Sciences
2025



Biological evaluation of bioengineered precision antimicrobial nanoparticles for gastric infection

Clara Pinto Bessa

Dissertation carried out as part of the Master in Biochemistry,
Department of Chemistry and Biochemistry,
2025

Supervisor
Paula Parreira, PhD, Associate Researcher, Institute for Research and Innovation in Health (i3S)

Co- Supervisors
Flávia Castro, PhD, Junior Researcher, Institute for Research and Innovation in Health (i3S) and M. Cristina L. Martins, PhD, Group Leader, Institute for Research and Innovation in Health (i3S) (i3S/ICBAS)

INSTITUTO
DE INVESTIGAÇÃO
E INOVAÇÃO
EM SAÚDE
UNIVERSIDADE
DO PORTO

Acknowledgements

Fazer um mestrado foi, sem dúvida, uma das experiências que mais me transformaram como pessoa. Apesar de todo o trabalho e esforço envolvidos, sinto que cresci imensamente, tanto a nível pessoal como profissional.

Até ao início do estágio, os estudos, as cadeiras e os trabalhos académicos mantinham-se dentro de um certo nível de exigência. No entanto, começar o estágio no i3S, num grupo repleto de pessoas incríveis como o BeSurf, mudou-me por completo, e para melhor!

Quero começar por agradecer à minha orientadora, Paula Parreira, de sempre e para sempre minha amiga, uma verdadeira inspiração. Uma mulher capaz de fazer mil e uma coisas, sempre com um sorriso no rosto e uma boa disposição contagiante.

À minha coorientadora, Flávia Castro, que me acompanhou desde o início do estágio e partilhou comigo os seus conhecimentos com paciência e alegria: agradeço profundamente a orientação, a confiança depositada em mim e o apoio constante ao longo desta jornada.

À Cristina Martins, também minha coorientadora e líder do grupo BeSurf, uma pessoa com um conhecimento vastíssimo, sempre disposta a ajudar em qualquer questão. Obrigada por incentivar a participação em congressos, a procurar experiências no estrangeiro, a criar novas relações e a enfrentar desafios que, no início do estágio, me pareciam assustadores, mas que hoje encaro com entusiasmo e curiosidade.

Ao grupo BeSurf como um todo: agradeço não só pelas reuniões semanais, que me permitiram expandir o conhecimento para além da minha própria investigação ao conhecer os trabalhos dos meus colegas, mas também pelos almoços, lanches e momentos de convívio que ajudaram a aliviar o stress do dia a dia. Obrigada pelos passeios, palestras e todo o tempo partilhado durante o meu estágio. A todos, o meu profundo obrigado por estarem presentes nesta fase tão marcante.

À Beatriz, à Sofia e à Susana, investigadoras incríveis que tive o privilégio de conhecer durante o meu percurso na cultura celular: muito obrigada pela vossa disponibilidade, carinho e ajuda, que tanto me ensinaram.

À minha família, aos meus pais e ao meu irmão, que, mesmo sem compreenderem muito sobre a minha área de formação, sempre me apoiaram e incentivaram a seguir em frente. Ao resto da família, primos e tios, que sempre perguntavam com carinho

sobre o progresso da tese e demonstravam tanto orgulho no meu trabalho, deixo o meu mais sincero agradecimento. O vosso apoio deixou-me profundamente feliz.

Aos meus amigos, Lena, Miguel, Vitor, Ana e Joana, que, tal como eu, embarcaram na aventura de fazer o mestrado, ainda que em áreas distintas. O nosso espírito de entreajuda permaneceu intacto, e, apesar de nos vermos menos frequentemente por causa da vida profissional, a nossa amizade mantém-se firme e forte.

Por fim, agradeço a toda a comunidade do i3S, da FCUP e do ICBAS, que me proporcionaram as ferramentas e oportunidades para chegar até aqui. Sinto-me genuinamente orgulhosa por ter podido aprender e crescer tanto nestas instituições.

Resumo

A infeção crónica por *Helicobacter pylori* (*H. pylori*) está associada ao desenvolvimento de cancro gástrico. As terapias atualmente disponíveis, baseadas em antibióticos, apresentam elevadas taxas de insucesso, atingindo até 40% dos casos, o que reforça a necessidade de novas abordagens terapêuticas.

Para sobreviver, o *H. pylori* tem de extrair colesterol das células gástricas e incorporá-lo na sua membrana, um processo que desestabiliza as jangadas lipídicas e desencadeia uma resposta inflamatória exacerbada. Estudos prévios demonstraram que a bactéria reconhece colesterol imobilizado em superfícies de ouro e sofre lise ao interagir com nanopartículas (NP) de ouro funcionalizadas com colesterol. Com base neste estudo de prova de conceito, foram formuladas NP de quitosano conjugado com grupos norborneno (NorChit), posteriormente funcionalizadas com colesterol (Chol-NP). As Chol-NP foram produzidas através de um sistema de microfluídica, obtendo-se uma concentração na ordem de grandeza de 10^{10} NP/mL. A concentração e o diâmetro hidrodinâmico das NP foram determinados por Análise de Rastreamento de Partículas (NTA).

As Chol-NP demonstraram ser citocompatíveis em linhas celulares gástricas e em macrófagos, além de não apresentarem atividade hemolítica. A sua capacidade de induzir polarização (M1 ou M2) em macrófagos humanos foi avaliada por citometria de fluxo, analisando a expressão dos marcadores CD163, CD206, CD86, CD40 e HLA-DR. Os resultados mostraram que as Chol-NP não alteraram significativamente a expressão destes marcadores, sugerindo que estas NP são imuno-seguras.

Em conjunto, estes resultados reforçam as Chol-NP como uma estratégia promissora no combate à infeção por *H. pylori*, promovendo a continuação do seu desenvolvimento.

Palavras-chave: Biocompatibilidade, *Helicobacter pylori*, Resposta Imune, Nanopartículas de Quitosano.

Abstract

Chronic *Helicobacter pylori* (*H. pylori*) infection is strongly associated with the development of gastric cancer. Currently available antibiotic-based therapies have high failure rates, reaching up to 40% of cases, reinforcing the need for new therapeutic approaches.

To survive, *H. pylori* relies on the uptake of cholesterol from gastric cells and its incorporation into the membrane, a process that destabilizes the lipid rafts and triggers an exacerbated inflammatory response. Previous studies have shown that the bacterium recognizes cholesterol immobilized on gold surfaces (2D) and undergoes lysis upon interacting with cholesterol-functionalized gold nanoparticles (NP, 3D). Based on this proof-of-concept study, chitosan NP conjugated with norbornene groups (NorChit) were designed and subsequently functionalized with cholesterol (Chol-NP). The Chol-NP were produced using a microfluidic system, achieving a concentration in the order of magnitude of 10^{10} NP/mL. The concentration and hydrodynamic diameter of the NP were determined by Nanoparticle Tracking Analysis (NTA).

Chol-NP were cytocompatible with gastric cell lines and macrophages, as well as non-hemolytic. Their ability to induce polarization (M1 or M2) in human macrophages was assessed by flow cytometry, analyzing the expression of the markers CD163, CD206, CD86, CD40, and HLA-DR. The results showed that Chol-NP did not significantly alter the expression of these markers, suggesting that these NP are immunosafe.

Taken together, these results further support the development of Chol-NP as a promising strategy to counteract *H. pylori* infection.

Keywords: Biocompatibility, Chitosan Nanoparticles, *Helicobacter pylori,* Immune Response.

Table of Contents

List of Tables viii

List of Figures ix

Abbreviations x

I. Introduction 1

1. Overview of *Helicobacter pylori* 2

1.1 *H. pylori:* Discovery and Main Characteristics 2

1.2 Pathologies caused by *H. pylori* infection 3

1.3 Diagnosis and prevalence 4

1.4 Virulence and Colonization Factors 6

2. *Helicobacter pylori* evasion and modulation of the host immune system 8

2.1 Recognition of *H. pylori* by the immune system 8

2.2 Strategies of *H. pylori* for evading innate and adaptive immunity 8

2.3 Biological consequences of cholesterol extraction - immune evasion and inflammation 11

2.4 Macrophage polarization and gastric damage 12

3. Therapeutic approaches for *Helicobacter pylori* infection 14

3.1 Conventional treatment 14

3.2 Alternative therapeutic strategies 15

3.3 Bioengineered strategies 16

3.3.1 Chitosan-based micro- and nanoparticles 19

II. AIM 23

III. Material and Methods 25

1. Microfluidic System 26

2. Norbornene-modified chitosan (NorChit) 27

3. Norbornene Chitosan Nanoparticles (NC-NP) and Cholesterol Nanoparticles (Chol-NP) production 27

4. Nanoparticle Characterization 29

5. Nanoparticles cytotoxicity studies 29
5.1 Cell lines 29
5.1.1 Culture……..……..29
5.1.2 Metabolic activity assay 32
5.2 Macrophages……..…31
5.2.1 Isolation of Human Monocytes……..…31
5.2.2 Cell seeding and metabolic activity assay……31
6. Nanoparticles hemocompatibility study……32
7. Macrophage profile evaluation upon exposure to nanoparticles 33
8. Statistical analysis 35
IV. Results and Discussion 37
1. Nanoparticles (NP) characterization 38
2. Cyto- and hemocompatibility of Cholesterol nanoparticles (Chol-NP) and NorChit nanoparticles (NC-NP) 39
2.1 Cytocompatibility in gastric cell lines 39
2.2 Hemocompatibility in Reb Blood Cells (RBCs) 41
2.3 Cytocompatibility in human macrophages 42
3. Macrophage profile evaluation 45
3.1 Evaluation of the expression profile of CD163 and CD206 46
3.2 Evaluation of the expression profile of CD86, CD40 and HLA-DR 49
V. Conclusions and Future work 53
VI. References 56

List of Tables

Table 1 Summary of *Helicobacter pylori* mechanisms of immune evasion via pattern recognition receptors (PRRs). 9
Table 2 Most common classes of microparticles (MP) and nanoparticles (NP) 17
Table 3 Nanoparticles characterization 38

List of Figures

Figure 1 - Schematic representation of *Helicobacter pylori* cell wall structure..... 2
Figure 2 - Summary representation of immune and inflammatory response after *Helicobacter pylori* infection 4
Figure 3 - Global map of the prevalence of *Helicobacter pylori* infection 5
Figure 4 - Structure and virulence factors of *Helicobacter pylori*..... 6
Figure 5 - Schematic representation of how *Helicobacter pylori* is recognized, triggering an A) innate and B) adaptive immune response..... 11
Figure 6 - Macrophage polarization: M1 and M2 subtypes 13
Figure 7 - Norbornene groups conjugation onto chitosan 20
Figure 8 - Schematic representation of nanoparticle (NP) production in a microfluidic system using NorChit and a thiolated molecule for conjugation 20
Figure 9 - Schematic representation of the designed microfluidic system..... 26
Figure 10 - Schematic representation of the production of Cholesterol Nanoparticles (Chol-NP) 28
Figure 11 - A) Gating strategy used to evaluate macrophage polarization; B) Polarization profile of monocytes..... 35
Figure 12 - Metabolic activity of A) AGS and B) MKN28 cell lines 40
Figure 13 - Hemolysis assay 42
Figure 14 - Metabolic activity of human macrophages..... 43
Figure 15 - Phenotype of macrophages A) before and B) after being stimulated with Cholesterol nanoparticles (Chol-NP) or C) with NorChit nanoparticles (NC-NP) at NP concentrations in the order of magnitude of 10^{10} NP/mL 44
Figure 16 - Effect of Cholesterol-nanoparticles (Chol-NP) and NorChit-nanoparticles (NC-NP) on human macrophages polarization..... 45
Figure 17 - Surface marker expression is presented as scatter plots for A) CD163 and B) CD206, and the corresponding percentage of positive cells (% Cells) in C) and D), from human macrophages. Median fluorescence intensity (MFI) of E) CD163 and F) CD206 47
Figure 18 - Surface marker expression shown as scatter plots for A) CD86, B) CD40, and C) HLA-DR, and corresponding expression frequencies (% Cells) in D), E), and F), in human macrophages. Median fluorescence intensity (MFI) for G) CD86, H) CD40, and I) HLA-DR 50

Abbreviations

^{1}H NMR – Proton Nuclear Magnetic Resonance

AGS – Human gastric adenocarcinoma cell line

AMPs – Antimicrobial Peptides

AP-1 – Activator Protein-1

APC – Antigen-presenting cells

ATR-FTIR – Attenuated Total Reflection – Fourier Transform Infrared Spectroscopy

BabA – Blood group antigen-binding adhesin A

CagA – Cytotoxin-associated protein A

CCL(17) – Chemokine (C-C motif) ligand (17)

CCL(3) – Chemokine (C-C motif) ligand (3)

CD(14) – Cluster of Differentiation (14)

Cgt –Cholesterol-α-glucosyltransferase

Chol – Thiol- polyethylene glycol$_{75}$ -cholesterol

Chol-NP – Nanoparticles functionalized with Chol

CHSJ –Centro Hospitalar São João

COX2 – Cyclooxygenase-2

CS – Chitosan

CuAAC – Copper-catalyzed Azide-Alkyne Cycloaddition

DC – Dendritic Cells

DLS – Dynamic Light Scattering

DMF – *N*,*N*-Dimethylformamide

DNA – Deoxyribonucleic Acid

EGFR – Epidermal Growth Factor Receptor

EMT – Epithelial-Mesenchymal Transition

FACS – Fluorescence-Activated Cell Sorter

FDA – Food and Drug Administration

FTIR – Fourier Transform Infrared Spectroscopy

GC – Gastric Cancer

Hb – Hemoglobin

HLA-DR – Human Leukocyte Antigen– DR isotype

HPLC – High Performance Liquid Chromatography

IARC – International Agency for Research on Cancer

IFN-(β) – Interferon (beta)

IL-(10) – Interleukin-(10)

iNOS – Inducible nitric oxide synthase

IRF3 – Interferon regulatory factor 3

JAK/STAT1 – Janus kinase/Signal Transducer and Activator of Transcription 1

LD – Live/Dead stain

LF – Lactoferrin

LPS – Lipopolysaccharide

MALT – Mucosa-Associated Lymphoid Tissue lymphoma

MAPK – Mitogen-Activated Protein Kinase

M-CSF – Macrophage Colony Stimulating Factor

MFI – Mean Fluorescence Intensity

MHC – Major Histocompatibility Complex

MKN28 – Human gastric adenocarcinoma cell line

MPs – Microparticles

MS – Mass Spectrometry

NF-κB – Nuclear factor kappa-B

NLRs – NOD-like receptors

NO – Nitric Oxide

NOD1 – Nucleotide-binding Oligomerization Domain-containing protein 1

NorChit – Norbornene-modified chitosan

NP – Nanoparticles

NTA – Nanoparticle Tracking Analysis

OMP – Outer Membrane Protein

OMVs – Outer Membrane Vesicles

P38 – Protein kinase

PAMPs – Pathogen-Associated Molecular Patterns

PBMC – Peripheral Blood Mononuclear Cells

PBS – Phosphate Buffered Saline

PDI – Polydispersity Index

PDMS – Polydimethylsiloxane

PEG – Polyethylene Glycol

Pen/Strep – Penicillin/Streptomycin

PFA – Paraformaldehyde

PPI – Proton Pump Inhibitor

PRRs – Pattern Recognition Receptors

RBC – Red Blood Cells

RIG1 – Retinoic Acid-Inducible Gene I

RNS – Reactive Nitrogen Species

ROS – Reactive Oxygen Species

RPMI – Roswell Park Memorial Institute medium

RT – Room Temperature

SabA – Sialic acid-binding adhesin

SD – Standard deviation

SPAAC – Strain-Promoted Azide-Alkyne Cycloadditions

STING – Stimulator of Interferon Genes

TC – Tissue Culture

TGF-β – Transforming Growth Factor beta

TLR – Toll-Like receptor

TNF-(α) – Tumor Necrosis Factor-(alpha)

TRIM30a – Tripartite Motif Containing 30 Alpha

Th(1) – T helper type 1 cells

Treg – Regulatory T cells

TSA – Tryptic Soy Agar

T4SS – Type IV Secretion System

UBT – Urease Breath Test

US – Unstained sample

UV – UltraViolet radiation

VA-086 – 2,2′-azobis[2-methyl-*N*-(2-hydroxyethyl) propionamide

VacA – Vacuolating cytotoxin A

VEGF – Vascular Endothelial Growth Factor

I. Introduction

1. Overview of *Helicobacter pylori*

1.1 *H. pylori:* Discovery and main characteristics

For many years, the stomach was considered an inhospitable environment for microorganisms due to its acidic nature. However, this changed in 1983, after the successful isolation and culture of *Helicobacter pylori* (*H. pylori*) by Barry Marshall and Robin Warren [1]. Marshall and Warren observed the bacterium in samples from patients with gastric inflammation and correlated this clinical observation with the presence of the pathogen in the body and its clinical manifestations. To prove their hypothesis, Marshall ingested the bacterium, developed gastritis, and cured himself using antibiotics, demonstrating the link between *H. pylori* and gastric infection. This discovery earned Marshall and Warren the Nobel Prize in Physiology in 2005 [2].

H. pylori is a Gram-negative bacterium and microaerophilic bacterium, as it requires less than 5% O_2 for optimal growth, and is mainly found in the pyloric region of the stomach [3]. Its cell wall is composed of an inner and outer membrane separated by the periplasmic space [4] (***Figure 1***). It possesses a peptidoglycan layer, known as murein which, after being analyzed by high-performance liquid chromatography (HPLC) and mass spectrometry (MS), revealed a unique amino acid composition, very distinct from other Gram-negative bacteria.

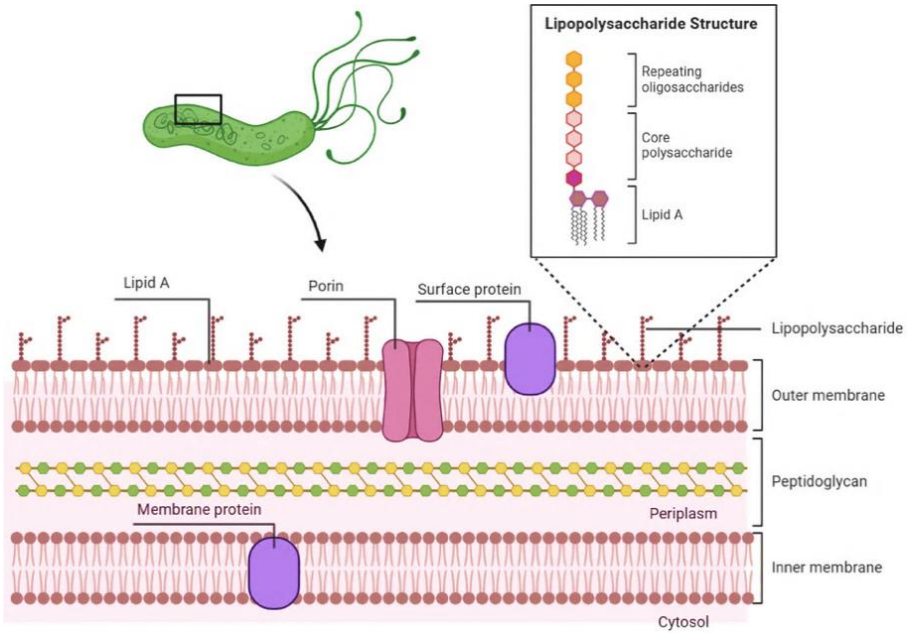


***Figure 1. Schematic representation of Helicobacter pylori* cell wall structure**. Image created using *Biorender.com* (not to scale).

These differences provide greater flexibility to the cell, facilitating its movement through the gastric environment and allowing the bacteria to undergo changes in shape

(morphological plasticity) [5], being able to exhibit either a bacillus (“S” shaped) or a coccoid morphology, a non-metabolically active state that is associated to stress conditions, as antibiotics exposure or nutrient starvation [6]. When in its bacillar morphology, *H. pylori* has approximately 0.5 to 1 μm in width and 2 to 4 μm in length and features 4 to 6 unipolar flagella covered by a characteristic sheath, essential for this extracellular pathogen to cross the gastric mucus layer and reach the surface of epithelial cells, where it establishes infection [7, 8].

1.2 Pathologies caused by *H. pylori* infection

Upon infection*, H. pylori* infection elicits a strong immune and inflammatory response that may cause several pathologies, as chronic gastritis, gastric ulcers and, in approximately 2% of infected individuals, gastric cancer (GC), the fifth most common and deadliest cancer worldwide [9], with a 5-year survival rate of less than 20% [10]. *H. pylori* infection is also linked to 92-98% of Mucosal Associated Lymphoid Tissue (MALT) lymphoma cases. In 1994, it was classified as a class 1 human carcinogen by the International Agency for Research on Cancer (IARC) and, to date, remains the only known carcinogenic bacterium [11].

The *H. pylori*-induced inflammatory process (***Figure 2***) begins with an increased recruitment of inflammatory cells, which play a key role in triggering the release of reactive oxygen species (ROS), degradative enzymes and pro-inflammatory cytokines [12]. The accumulation of these molecules progressively induces cellular damage and disturbs the local gastric microenvironment (commonly associated with gastritis and ulcers), eventually triggering epithelial-to-mesenchymal transition (EMT) in epithelial cells [13], which become potential tumor precursor cells [14].

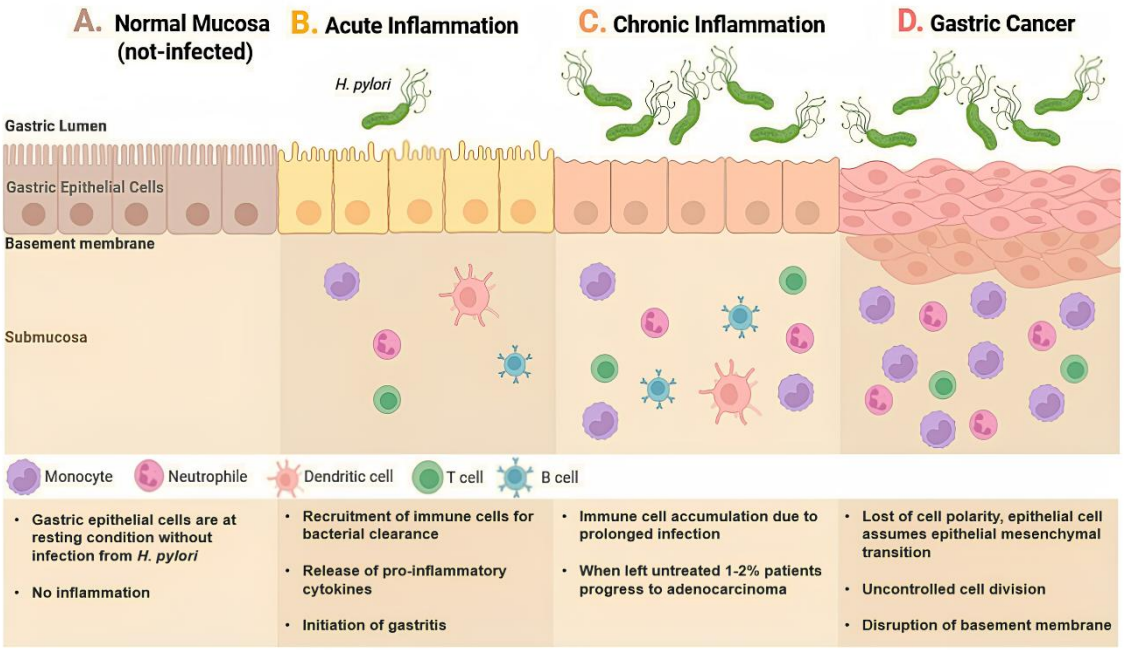


Figure 2. **Summary representation of immune and inflammatory response after *Helicobacter pylori* infection. A)** Uninfected gastric epithelial cells show no sign of inflammation; **B)** Upon *H. pylori* infection, inflammation of the gastric mucosa (gastritis) occurs; **C)** Ineffective bacterial clearance leads to prolonged infection and continuous recruitment of immune cells, resulting in chronic inflammation; **D)** Depending also on genetic and environmental factors, approximately 1–2% of the patients will undergo further cellular changes and disease will progress to gastric cancer. Image adapted from [8] using *Biorender.com.*

The carcinogenic process that subsequently occurs is described by the Correa´s Cascade [15]. This chain of events describes the histopathological changes provoked by *H. pylori* infection in the gastric mucosa, starting with chronic gastritis, progressing to gastric atrophy, followed by metaplasia and dysplasia, being gastric cancer the last stage [16]. These cellular changes are also driven by bacterial virulence factors, such as toxins, and by mechanisms involved in immune evasion and bacterial survival [17], including the extraction of cholesterol from the gastric epithelium [18], a process that will be discussed in detail in following sections.

1.3 Diagnosis and prevalence

The most common tests to diagnose *H. pylori* infection include:

(**a**) Urea Breath Test (UBT), in which the patient ingests a solution containing urea labelled with carbon isotopes. Then, if the molecule is hydrolyzed by the bacterium enzyme urease, the labelled carbon will be detected in the patient's exhalation (CO_2), confirming the infection [19];

(**b**) Serological tests that detect antibodies against *H. pylori*, although this method cannot distinguish between an active infection and a previously eradicated one [20];

(**c**) Stool antigen tests, which detect specific bacterial proteins in the feces [21];

(**d**) Endoscopy combined with a biopsy, allowing the physician to directly visualize the gastric mucosa and collect tissue samples to screen for other potential malignant lesions [22].

H. pylori infection occurs mainly in childhood and is common among family members that cohabit [3]. Infection is usually asymptomatic and can persist for life if left untreated [23]. Approximately 4 billion people are infected globally, being the heterogeneous worldwide distribution of *H. pylori* infection depicted in ***Figure 3***: in less developed countries, infection rates can reach 80-90% of the population, while more developed countries have lower prevalence rates, generally below 50% [23, 24]. This discrepancy may be related with the mechanism of transmission, as *H. pylori* is thought to mainly spread via oral-oral or fecal-oral transmission through contaminated water or food in areas where hygiene practices are inadequate [25]. Also, recent studies suggest that men have a higher infection rate than women [26].

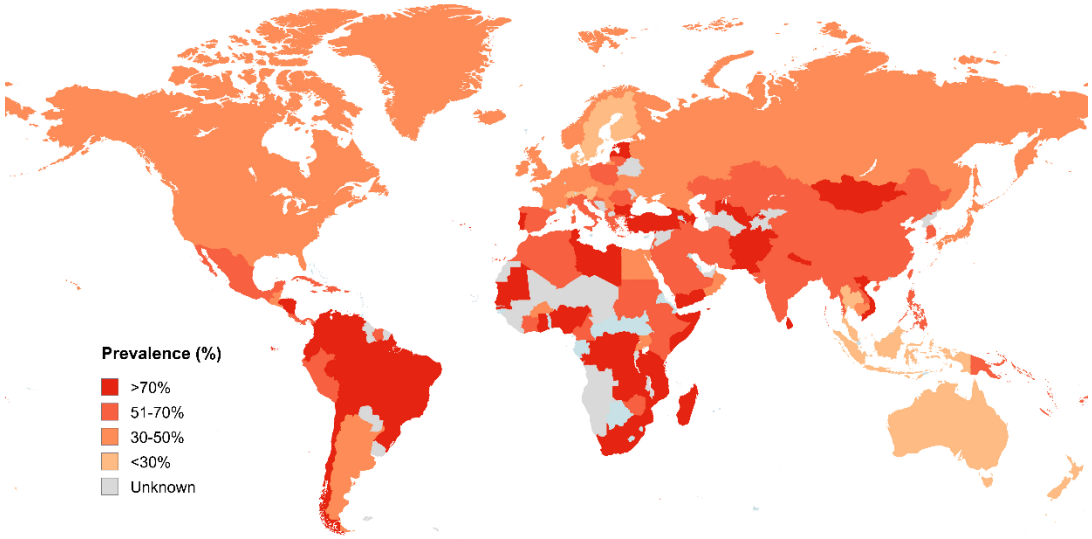


Figure 3. **Global map of the prevalence of *Helicobacter pylori* infection**. Countries shaded in darker red indicate higher prevalence rates, whereas lighter red tones represent low or negligible prevalence. Image adapted from [27] using *mapchart.net.*

Although classified as a developed country, Portugal ranks among the countries with the highest *H. pylori* prevalence worldwide, being estimated that over 60% of the Portuguese population carries the bacterium, with rates climbing to 84% in the North region [28].

1.4 Virulence and colonization factors

H. pylori has several mechanisms that enable its survival and allows it to efficiently colonize the gastric epithelium, which are summarized in ***Figure 4*** and explored below.

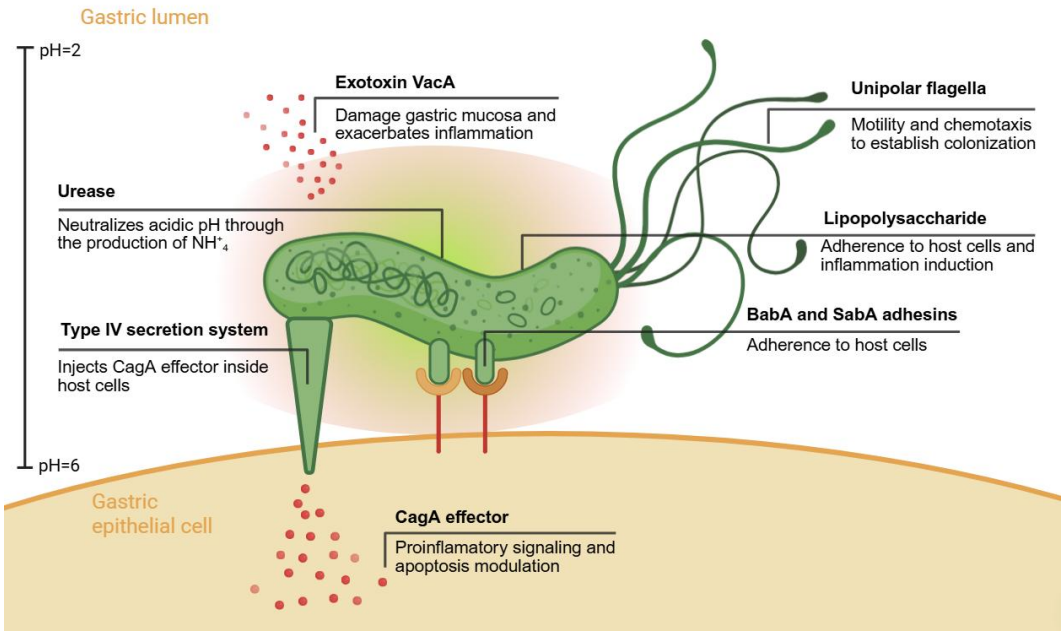


Figure 4. **Structure and virulence factors of *Helicobacter pylori***. Virulence factors such as flagella, urease, adhesins, lipopolysaccharide, CagA toxin, VacA toxin and CagA toxin injection system into the host cell via a type IV secretion system. Image adapted from [29] using *Biorender.com.*

Adhesion to gastric cells: Specific adhesion to the surface of gastric epithelial cells is possible due to several adhesive proteins (adhesins) expressed on the bacterium outer membrane, which are encoded by the Outer Membrane Protein (OMP) genes. Among them are the blood group antigen-binding adhesin (BabA) and the sialic acid-binding adhesin (SabA) that bind to the Lewis b and Lewis X receptors, respectively, present on the host gastric epithelium [30].

Survival in acidic environment: *H. pylori* can survive in the acidic environment (pH <4) of the stomach due to the enzyme urease. This enzyme catalyzes the hydrolysis of urea into carbon dioxide and ammonia, an alkaline product that not only neutralizes the microenvironment surrounding the bacterium, but also alters the viscosity of the gastric mucus layer, thereby facilitating its penetration and enabling *H. pylori* to reach the gastric epithelial surface, where infection is established [31, 32].

Morphological plasticity: *H. pylori* can also alter its bacillar morphology to a coccoid morphology (spherical shape) under stress conditions, such as nutrient deprivation or sublethal doses of antibiotics [33]. Coccoid form is a metabolically inactive form that

represents a “viable but non-culturable” state, wherein *H. pylori* can survive but does not grow *in vitro* when cultured. This makes the detection and treatment with conventional antibiotics, whose activity rely on active cellular processes, more challenging [34]. Additionally, this state facilitates the accumulation of toxic substances within the bacterium, which can be later released, further increasing its pathogenicity when it returns to its metabolically active form (bacillar) [33, 35].

Toxins: The production of protein toxins, such as the Cytotoxin-associated gene A (CagA) and Vacuolating cytotoxin A (VacA), contribute to the virulence of the bacteria and further promote cellular damage [36]. The cytotoxin associated with the gene *cagA* (CagA toxin), present in more pathogenic strains (type 1 strains, associated with poorer prognosis), is injected into epithelial cells through a type IV secretion system (T4SS). This toxin interferes with several intracellular signaling pathways, such as nuclear factor kappa-B (NF-κB) and epidermal growth factor receptor mitogen-activated protein kinase (EGFR-MAPK) pathways, eventually leading to cellular DNA damage [37]. In addition to protein effectors, the T4SS is also capable of delivering bacterial genetic material, such as DNA fragments, directly into host cells. This exogenous DNA can activate innate immune sensors, triggering pro-inflammatory responses [38]. The Vacuolating cytotoxin A (VacA toxin), encoded by the *vacA* gene, is present in all *H. pylori* strains [39]. This gene can encode different subtypes of these toxins, which are associated with a higher likelihood of developing peptic ulcers and gastric cancer [36]. This toxin is classified as pore-forming, inducing the formation of vacuoles that are absorbed by the cells and directed to the mitochondria, causing dysfunction of the organelles and apoptosis [40, 41]. Furthermore, it has been previously demonstrated that VacA increases Cyclooxygenase-2 (COX2) levels, which through positive feedback promotes the production of prostaglandins, leading to a robust immune response [42].

Outer Membrane Vesicles (OMVs): Another factor that facilitates *H. pylori* colonization and survival is the secretion of OMVs. OMVs are employed by *H. pylori* and other Gram-negative bacteria to exchange genetic material, signaling molecules and other compounds that facilitate communication, enhance pathogenicity, and potentially contribute to biofilm formation [43], thereby promoting more challenging conditions for the treatment [44].

Immune system evasion: The ability of *H. pylori* to evade the host immune system, either through antigenic disguise by mimicking host molecules, such as Lewis blood group antigens [45] or by expressing lower amounts of pro-inflammatory lipopolysaccharides (LPS) in its cell wall, as it will be discussed in the following sections, is one of the main

reasons for both the persistence of the bacterium and the difficulty in achieving therapeutic efficacy [46].

2. *Helicobacter pylori* evasion and modulation of the host immune system

2.1 Recognition of *H. pylori* by the immune system

Upon infection, the host immune system is primarily activated through pattern recognition receptors (PRRs), which are expressed by a variety of cells, including epithelial and immune cells [47]. PRRs are classified into several major families, including Toll-like receptors (TLRs), NOD-like receptors (NLRs), and RIG-I-like receptors (RLRs). Each group detects specific types of microbial or danger signals, either at the cell surface, in endosomal compartments or within the cytoplasm [48]. PRRs play a crucial role in detecting invading pathogens by recognizing conserved molecular signatures known as pathogen-associated molecular patterns (PAMPs), as well as damage-associated molecular patterns (DAMPs) released from stressed or dying host cells. PAMPs include components such as bacteria LPS, flagellin and nucleic acids, while DAMPs comprise host-derived DNA or RNA fragments, as well as mitochondrial DNA [17, 49]. In the case of *H. pylori*, TLRs and NLRs are particularly relevant. TLRs, such as TLR4 and TLR5, are located on the plasma membrane and are typically responsible for detecting extracellular bacterial components like LPS and flagellin [50].

Beyond surface receptors, intracellular receptors like NOD1 (a member of the NLR family) detect bacterial peptidoglycan delivered into epithelial cells. Upon activation, NOD1 initiates two parallel signaling cascades: one involving the transcription of the inflammatory protein 1 (AP-1) or the NF-κB transcription factor, which promotes the expression of pro-inflammatory cytokines and defensins, and another involving interferon regulatory factor 3 and 7 (IRF3/7) that leads to the production of type I interferons (e.g. IFN-β) [17]. These responses further amplify the innate immune response and contribute to mucosal inflammation.

2.2 Strategies of *H. pylori* for evading innate and adaptive immunity

Beyond the action of its virulence factors, the remarkable persistence of *H. pylori* in the human stomach is also attributed to its ability to evade the host immune system through various mechanisms [17, 51].

H. pylori exhibits molecular modifications in its LPS (in the lipid A domain) that weaken its detection by TLR4, being its flagellin also poorly recognized by TLR5 [52]. In addition, *H. pylori* is also capable of escaping immune recognition by other intracellular receptors, as summarized in ***Table 1***.

Table 1. **Summary of *Helicobacter pylori* mechanisms of immune evasion via pattern recognition receptors (PRRs).** Table adapted from [48].

PRR Type	PRR	PAMP Recognized	Mechanism of Immune Evasion by *H. pylori*	Ref
TLR	**TLR4** Plasma membrane receptor	Lipopolysaccharide (LPS)	Removal/modification of phosphate groups at 1′ and 4′ positions in lipid A, reducing TLR4 activation	[53]
TLR	**TLR5** Plasma membrane receptor	Flagellin (FlaA)	Divergent sequences in flagellin monomers reduce TLR5 recognition	[54]
TLR	**TLR9** Intracellular receptor (endosomes)	CpG DNA motifs	Suppression of IL-17 production to reduce inflammatory response and facilitate immune evasion	[55]
STING	**STING** Cytosolic sensor	Intracellular DNA	Upregulation of TRIM30a (STING suppressor) and downregulation of IRF3, impairing bacterial DNA sensing pathways	[56]
RLR	**RIG-I** Cytosolic sensor	Intracellular RNA	Downregulation of IRF3	[56]
NLR	**NOD1** Cytosolic sensor	Peptidoglycan	Deacetylation of peptidoglycan, reducing NOD1 recognition	[57]

DNA – Deoxyribonucleic Acid; FlaA – Flagellin; *IL-17 – Interleukin 17; IRF3 – Interferon Regulatory Factor 3; LPS – Lipopolysaccharide; NLR – NOD-like Receptor; NOD1 – Nucleotide-binding Oligomerization Domain-containing Protein 1; RIG-I – Retinoic Acid-Inducible Gene I; RLR – RIG-I-like Receptor; STING – Stimulator of Interferon Genes; TLR4 – Toll-like Receptor (4); TRIM30a – Tripartite Motif-containing Protein 30a.*

Although *H. pylori* initially evades some of the innate immune mechanisms (***Figure 5A***), partial detection through the processing of antigens presented by antigen-presenting cells (APCs), such as dendritic cells (DCs) and macrophages [49], results in the activation of the adaptive immune response, both cellular (T cell activity) and humoral (antibody production by B cells), which constitute the host second line of defense [17].

Macrophages primarily phagocytose pathogens or their components and release cytokines that act at the site of infection, amplifying the immune response. DCs, in turn, are responsible for migration to lymph nodes and the activation of naive T cells [58]. Within these lymph nodes, DCs drive the differentiation of naive T cells into $CD4^+$ and $CD8^+$ T cells, capable of recognizing molecules bound to the major histocompatibility

complex (MHC) class II and class I molecules, respectively [48]. This process marks the beginning of the adaptive immune response [46].

In a *H. pylori* infection scenario, T cells antigen presentation occurs predominantly via MHC class II molecules, leading to the differentiation of $CD4^+$ T cells mainly into T helper (Th)1, Th17 and regulatory T cells (Treg) (***Figure 5B***) [48]. Th1 cells produce pro-inflammatory cytokines, including interferon-γ (IFN-γ), tumor necrosis factor-β (TNF-β) and interleukin (IL)-2, which typically mediate immune responses against intracellular pathogens [59, 60] or, in the case of *H. pylori*, against bacterial toxins and antigens that gain access to host cells. Th17 cells, on the other hand, direct their immune response toward extracellular pathogens through the production of IL-17, contributing to inflammation associated with neutrophil infiltration [48], resulting in severe damage to the gastric mucosa [61]. Treg cells, in turn, regulate and suppress the inflammatory response mediated by Th1 and Th17 cells to prevent excessive tissue damage [48]. However, this immunoregulatory activity contributes to the persistence of *H. pylori* in the stomach, as chronic suppression of inflammation undermines the effectiveness of the immune response [62, 63]. Furthermore, *H. pylori* has been shown to attenuate the strong Th1 mediated pro-inflammatory response by promoting the differentiation of $CD4^+$ lymphocytes into Th2 cells (***Figure 5B***), thus hindering the pathogen elimination by the immune system [60, 64]. Although Th2 responses are generally associated with pro-inflammatory action against extracellular parasites, in the context of *H. pylori* infection these cells ultimately favor immune evasion by counteracting/regulating Th1-induced inflammation. Thus, *H. pylori* exploits the regenerative functions of Th2 associated cytokines, creating an illusory signal of repair and homeostasis that tricks the immune system into interpreting the gastric mucosa as recovering, despite the persistence of the infection. ***Figure 5B*** summarizes these adaptive immune processes during infection by the pathogen *H. pylori*, in addition to briefly explaining how the initial (innate) compromised detection occurs in the host (***Figure 5A***).

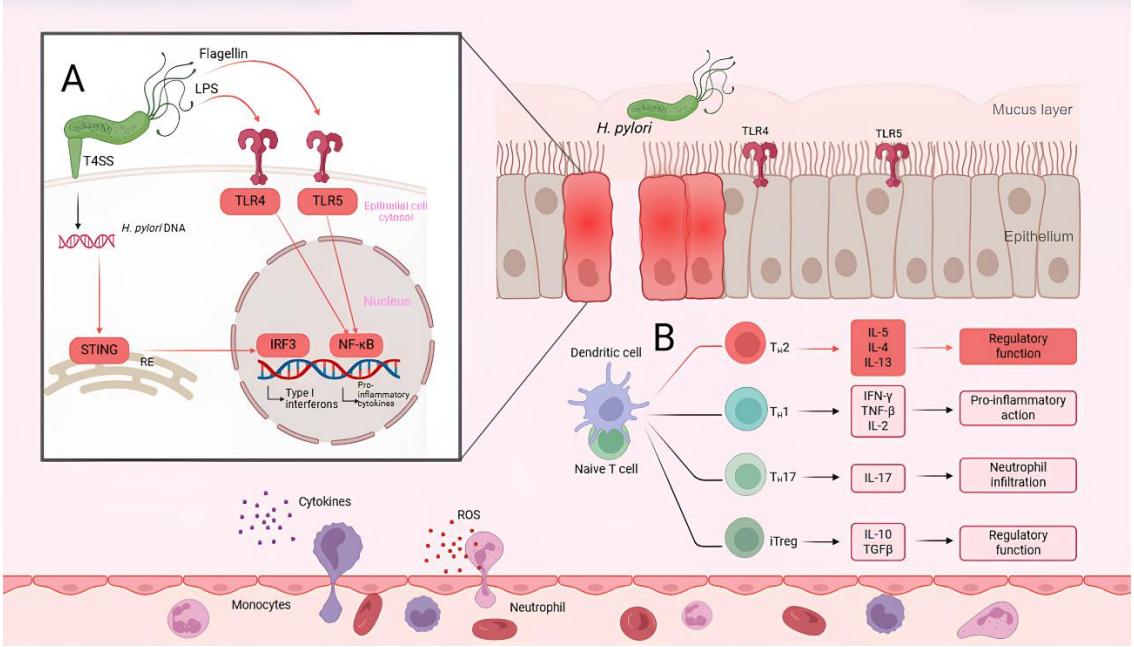


***Figure 5*. Schematic representation of how *Helicobacter pylori* is recognized, triggering an A) innate and B) adaptive immune response. A)** *H. pylori* prevents the initiation of pro-inflammatory cytokines production and type I interferon responses by reducing detection via TLR4 and TLR5 and by delivering its genetic material intracellularly through the type IV secretion system [17, 52, 53]. **B)** The differentiation of naive T cells into Th1 (pro-inflammatory) cells is attenuated by *H. pylori*, which promotes differentiation toward Th2 cells. [55, 56, 61]. *IRF3 – Interferon Regulatory Factor, NF-κB – Nuclear Factor kappa-light-chain-enhancer of activated B cells, ROS – Reactive Oxygen Species, STING – Stimulator of Interferon Genes, T4SS – Type IV Secretion System, TLR4 – Toll-like Receptor 4, TLR5 – Toll-like Receptor 5.* Image created using *Biorender.com.*

Although initially there is an intense inflammatory response that damages the epithelium, over time *H. pylori* can promote immune modulation to prevent elimination and maintain a chronic low-grade infection [60, 64].

2.3 Biological consequences of cholesterol extraction - immune evasion and inflammation

To survive *H. pylori* must extract cholesterol from the host cell membranes as it is unable to synthesize this molecule *de novo* (auxotrophic for cholesterol) [65]. *H. pylori* possesses the enzyme cholesterol-α-glucosyltransferase, which transforms the extracted cholesterol into cholesteryl glucosides that are subsequently incorporated into the cell membrane. This incorporation provides disguise to the immune system and increases bacterial resistance to antibiotics [66], either by physically protecting the bacterial membranes or by altering the membrane fluidity, which hinders the entry of drugs that target the cytoplasmic environment [67]. Furthermore, it has also been proven that an increased cholesterol-α-glucosyltransferase activity is directly related to the

worsening of gastric inflammation, since this enzyme is recognized by invariant natural killer T cells (distinct type of T cells of the innate immune system) [68]. Upon recognition of the cholesterol-derived glycolipids, natural killer T cells become rapidly activated and release large amounts of cytokines, resulting in the recruitment and activation of other immune cells [69].

On mammalian cells, cholesterol is mainly found in microdomains within cellular membranes known as lipid rafts [18, 70]. The cholesterol removal disrupts these lipid rafts where the IFN-γ receptors are located. These receptors are required for activating the Janus kinase/Signal Transducer and Activator of Transcription 1 (JAK/STAT1) signaling pathway [71], which is crucial for producing molecules that attract T cells as well as antimicrobial peptide producing cells [72], including neutrophils and epithelial cells, to the site of infection [73]. Thus, by blocking this pathway, *H. pylori* reduces the inflammatory response and evades the immune system, creating a protected environment for its survival [71]. The process of cholesterol extraction also promotes disruption of cell polarity, promoting to gastric carcinogenesis [74].

The cholesterol auxotrophy coupled with *H. pylori* positive chemotaxis toward this molecule makes cholesterol an appealing target for the development of new therapeutic strategies aimed at bacterial elimination [74].

2.4 Macrophage polarization and gastric damage

The *H. pylori*-induced exacerbated inflammatory response results from the infiltration of inflammatory cells, mainly neutrophils and monocytes that, upon entry in the tissue, differentiate into macrophages [75], as mentioned in ***Figure 5***. Neutrophils are the first cells to reach the site of infection where they actively release ROS. However, while neutrophils have a short lifespan and normally survive only a few hours [76], monocytes have a longer lifespan, allowing for a more sustained immune response [77]. When monocytic cells differentiate, the responses range from combating the initial infection to tissue regeneration. In addition, these phagocytic cells act as inflammatory mediators, as they are also capable of presenting bacterial antigens to T cells, representing a bridge between innate and adaptive immunity [78].

Circulating monocytes that reach the site of infection, following bacterial contact with the lamina propria, first differentiate into M0 macrophages, an intermediate, non-polarized state [79]. From this state, depending on the environment (tissue and stimuli), they can further polarize into M1-like (pro-inflammatory) or M2-like (anti-inflammatory)

phenotypes [80]. M1-like polarization is typically induced by pro-inflammatory stimuli such as IFN-γ, LPS, and Tumor Necrosis Factor-alpha (TNF-α), while M2 polarization is triggered by cytokines like IL-4, IL-13, IL-10, corticosteroids or transforming growth factor-β (TGF-β) [79-81] (***Figure 6***). This polarization is a crucial step, as it enables macrophages to adopt specialized functional roles, either amplifying the immune response and promoting antitumor activities and bacterial clearance (M1-like), or regulating inflammation and contributing to tissue repair and angiogenesis processes (M2-like) [82, 83]. The M2-like phenotype can be further subdivided into four subsets, based on the stimuli they respond to: M2a (induced by IL-4 and IL-13), M2b (induced by immune complexes and TLR ligands), M2c (induced by IL-10 and glucocorticoids), and M2d (induced by TLR agonists) [80] (***Figure 6***). These subtypes reflect the functional versatility of macrophages in different pathological and physiological contexts and represent a fundamental feature of innate immunity [84]. Nevertheless, the M1/M2 classification is a simplified model as *in vivo* macrophages exhibit a spectrum of overlapping activation states that vary with tissue context and immune challenge, and can be distinguished by specific surface markers and cytokine profiles [85, 86]. A proper balance between macrophage populations is essential for host homeostasis, as an imbalance favoring M1-like cells can lead to chronic inflammation and ultimately genomic instability [87], whereas a shift toward M2-like dominance can result in immunosuppression [86].

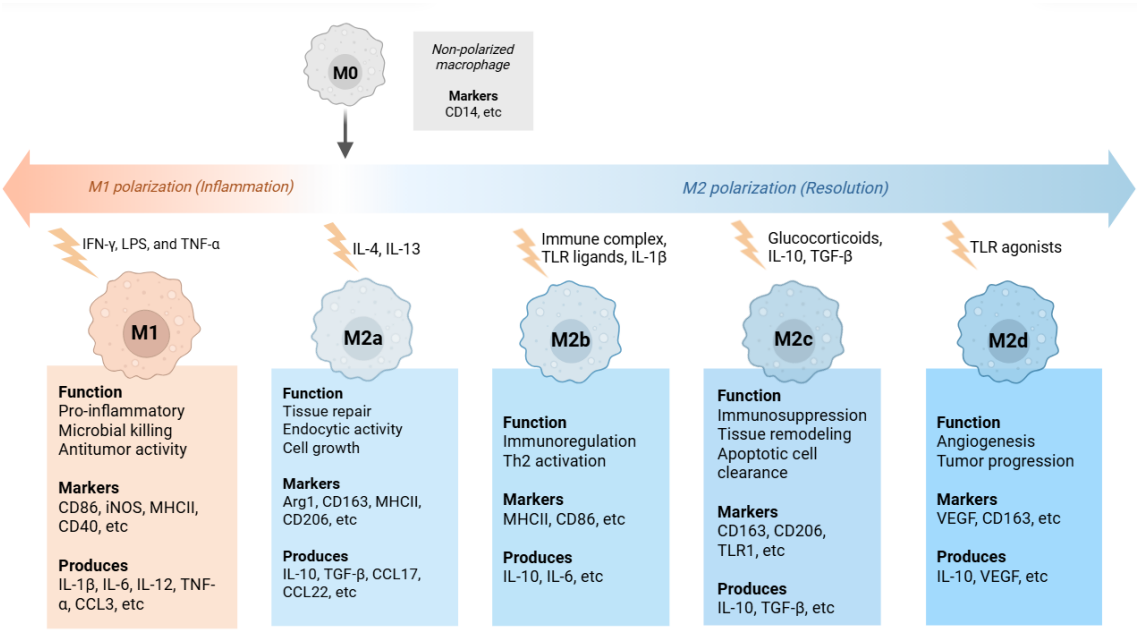


Figure 6. **Macrophage polarization: M1 and M2 subtypes**. Diagram illustrating the most reported surface markers, cytokines and polarization stimuli associated with each subtype [80, 88, 89]. Image created using *Biorender.com*. *CCL(17): C-C Motif Chemokine Ligand 17, CD(14): Cluster of Differentiation (14), IFN-γ: Interferon-gamma, IL-(1β): Interleukin-(1 beta), LPS: Lipopolysaccharide, MHCII: Major Histocompatibility Complex Class II, TGF-β: Transforming*

Growth Factor-beta, TLR: Toll-Like Receptor, TNF-α: Tumor Necrosis Factor-alpha, VEGF: Vascular Endothelial Growth Factor.

H. pylori can stimulate recruited macrophages to polarize towards the M1-like phenotype, leading to the production of pro-inflammatory factors that further exacerbate damage to the gastric mucosa, as demonstrated *in vitro* and *in vivo* [90]. A notable example is the chemokine CCL3, whose role has been described *in vitro*. CCL3 secretion during infection induces phosphorylation of p38, a member of the MAPK kinase family, leading to the disruption of tight junction proteins and compromising the integrity of the gastric epithelial barrier. These effects are mediated by inflammatory signaling, since CCL3 was also shown to stimulate the expression of pro-inflammatory factors in gastric epithelial cells, in addition to promoting their apoptosis and inhibiting cell proliferation [91]. Such structural destabilization of the epithelium is a recognized feature of tumors associated with *H. pylori* infection [3].

Furthermore, the increased expression of inducible nitric oxide synthase (iNOS), a hallmark of M1-like macrophages (***Figure 6***), plays a significant role in tissue damage. Excess nitric oxide (NO) production leads to its reaction with ROS, resulting in the formation of peroxynitrite ($ONOO^-$), a highly cytotoxic molecule [92]. This process has been associated with several pathological conditions, including gastritis [93], and constitutes an indirect mechanism through which the bacteria promote oxidative stress [94]. In parallel, direct mechanisms also contribute to this process, such as bacterial metabolic byproducts, namely hydrogen peroxide and superoxide, or the action of virulence factors, like CagA and VacA, which stimulate intracellular ROS production in epithelial cells [95].

In summary, the direct and indirect actions of both immune cells and bacterial virulence factors, such as CagA and VacA, collectively promote a microenvironment conducive to genomic instability and gastric disease progression.

3. Therapeutic approaches for *Helicobacter pylori* infection

3.1 Conventional treatment

Conventional treatment is based on a combination of broad-spectrum antibiotics and acid suppressive drugs (proton pump inhibitors (PPI) or H_2 antagonists) that are used to stabilize and boost the efficacy of the antibiotics in gastric settings, as these compounds increase the stomach pH [96, 97].

The treatment regimen is usually chosen empirically, based on regional patterns of bacterial resistance, local recommendations and drug availability [96, 98]. The current therapeutic gold standard in Europe is the Quadruple Therapy, that combines the use of Bismuth Subsalicylate salts with a PPI and the broad-spectrum antibiotics Tetracycline and Metronidazole for 10 days [99, 100]. Bismuth, administered orally in the form of salts, has a specific antimicrobial effect against *H. pylori* as it interferes with the bacterial cell wall and enzymes. In addition, this compound forms a protective layer over gastric ulcers and other gastric lesions to promote healing, while also preventing *H. pylori* from adhering to the gastric epithelium [52]. However, the available antibiotic based therapies present several associated problems, such as high rates of resistance, resulting in ineffective treatments that further contribute to the antimicrobial resistance crisis [101]. Additionally, the antibiotics lead to severe side effects that reduce patient adherence to the prescribed treatment, as well as to dysbiosis, with these alterations in the gastrointestinal microbiota affecting metabolism, hormonal secretion, and immune system modulation [59, 102].

There is also absence of an effective vaccine, mostly due to the bacterium ability to circumvent the host immune system [103]. This, coupled with high and increasing antibiotic resistance rates and the often recurrence of infection [23], are some of the factors that support the need for new therapeutic approaches.

3.2 Alternative therapeutic strategies

Probiotics: Probiotics, such as *Lactobacillus* sp. and *Bifidobacterium* sp., have demonstrated to reduce treatment-related side effects, including nausea and diarrhea, contributing to patient compliance to the therapeutic scheme, therefore enhancing eradication rates [104, 105]. However, probiotics are only considered adjuvants to conventional therapies.

Phytocompounds: Several plant-derived extracts have demonstrated inhibitory effects on *H. pylori* colonization, including extracts from *Pistacia lentiscus*, *Brassica oleracea*, and *Glycyrrhiza glabra*, which have shown promising results in *in vivo* studies [107]. These effects are mainly attributed to the presence of various bioactive molecules with antimicrobial properties [106]. For example, flavonoids such as quercetin and catechins, have shown the ability to inhibit urease activity, thereby impairing *H. pylori* survival in the gastric environment and colonization capacity [107]. Although supplementation with probiotics and/or phytocompounds are promising options, none of these have achieved

similar or better performance than the antibiotic therapy in reducing the bacterial burden or even clearing infection [3, 108]. Yet, their potential synergistic effects with conventional antibiotics may be further explored to enhance eradication rates and reduce treatment-related side effects [109].

Lactoferrin (LF): Studies have reported that this protein shows potential against *H. pylori* infection due to its anti-inflammatory properties [110]. Still, LF is considered an adjuvant and does not replace standard antibiotic therapy, primarily due to its low gastric stability, being susceptible to processes such as oxidation and/or hydrolysis [111, 112].

Phage therapy: To date there are no studies specifically applying it to the management of *H. pylori* infection [110, 113].

3.3 Bioengineered strategies

The major developments in the bioengineering field over the last decade have provided new strategies for gastric delivery, specifically by designing tailored micro- and nano-based systems for gastric settings. These systems can protect therapeutic compounds from the acidic environment of the stomach and transport them to be released at the site of infection, ultimately improving their bioavailability. Micro- (MP) and nanoparticles (NP), can be divided and classified based on their composition, which may include polymers, metals or lipids [112]. MP and NP physicochemical properties can be changed by altering their size and/or morphology [114]. In comparison with MP, NP have a higher surface area relative to their volume.

Table 2. **Most common classes of microparticles (MP) and nanoparticles (NP) developed for gastric settings**, their main components, and key features that make them suitable for the gastric environment. Table adapted from [112].

Class		Biomaterial	Properties	Ref
Polymeric		Chitosan	Mucoadhesive Antimicrobial	[115, 116]
		Polylactic-co-glycolic acid (PLGA)	Biocompatible Optimal control of drug release *in vivo* Adequate for several active ingredients	[117]
		Gliadin	Mucoadhesive	[118]
Lipidic		Lipids (e.g. phosphatidyletha nolamine)	Biocompatible Adequate for lipophilic and hydrophilic drugs, Easily modified to obtain mucoadhesive properties	[119]
Metallic		Gold	Antimicrobial Antitumor Mucoadhesive Used in theragnostic applications	[120, 121]
Others	Nanomicelles	Several (e.g. hyaluronic acid, chitosan)	Biocompatible pH-responsive Mucoadhesive Adequate for hydrophobic drugs	[121, 122]
	Nanocomposites	Several (e.g. polymeric or metallic nanoparticles)	Multiphase nanomaterial Combine different nanoparticles and their properties Accumulate the advantages of all the nanoparticles involved	[123]

Over the last years, several bioengineered therapies targeting *H. pylori* infection have been developed, exhibiting bactericidal or bacteriostatic activity [112]. For instance, approaches based on: (**a**) tampering with the adhesion of the bacterium to the host gastric cells; (**b**) selective drug release within the bacterium; or (**c**) binding to the *H. pylori* membrane for localized delivery of antimicrobial compounds have been explored. Highlighting strategy (**a**) are the MP developed by Gonçalves *et al*. functionalized with the Leb and sLex glycans that are expressed on gastric epithelial cells and recognized by the bacterial adhesins BabA and SabA, respectively. These MP contended for bacterial adhesion and were able to decrease the number of bacteria adhered to the gastric mucosa [124]. Regarding the selective drug release within the bacterium (approach (**b**)), an example is the work performed by Jing *et al*., who developed pH-sensitive NP conjugated with ureido groups, designed to encapsulate antibiotics or

bioactive compounds [125]. These NP exploited the UreI urea channel located in the membrane of *H. pylori*, which selectively transports urea into the bacterial cytoplasm under acidic conditions. Drug release occurs preferentially in acidic environments such as the stomach, allowing the NP to activate only when near or inside the bacterium, thereby enhancing therapeutic efficacy and minimizing side effects. Recognition by the UreI channel facilitates NP uptake into the bacterial cytoplasm, promoting selective intracellular drug delivery [125]. Although targeted drug delivery through the UreI channel has shown promise in increasing antibiotic uptake by *H. pylori*, its efficacy may be limited by competition from host-secreted urea and by channel closure at neutral pH, caused by ammonia production when the bacteria are attached to the epithelium [125]. Therefore, this strategy may be more suitable for preventive use in the mucus layer, before the bacteria reach the gastric epithelium [112]. Finally, strategy (**c**) involves the binding of pathogen-eradicating agents that recognize and specifically bind to the bacterial membrane. Two types of targets have been identified: non-specific targets, which are components of the *H. pylori* cell membrane and are also found in other bacteria, such as dextran sulfate, a membrane-associated polysaccharide; and specific targets, which rely on the use of antibodies [112].

Phototherapy and sonodynamic therapy are two examples of approaches that already exist on their own [126], but when combined with antibody-coated NP, improve *H. pylori* eradication. In phototherapy with NP, radiation is directed at specific wavelengths, selectively destroying bacteria without damaging surrounding tissues [130], thus overcoming one of the limitations of the traditional method [126]. Specific binding to bacteria is possible due to the use of polyclonal antibodies [127]. Sonodynamic therapy with NP containing antibodies or sonosensitizers, when activated by ultrasound, generates ROS with bactericidal effects. These NP can also be functionalized to sequester soluble bacterial toxins, such as VacA, further increasing their therapeutic potential [128].

Of the possible biomaterials to develop new strategies for gastric settings (***Table 2***), chitosan-based particles are the most appealing. The following section explores the physicochemical properties of chitosan (CS) and its application in the design and production of effective NP systems.

3.3.1 Chitosan-based micro- and nanoparticles

CS is a natural polymer obtained through the deacetylation of chitin found in the exoskeleton of crustaceans, insects, and cell wall of some fungi [129]. This material is non-toxic and is approved by the Food and Drug Administration (FDA) for oral administration [130], making it a preferred alternative to metals for the production of NP designed for oral delivery [108, 131]. Further, its cationic and hydrophilic nature facilitates interaction with cell membranes, enabling a more efficient *in situ* delivery of therapeutic compounds [132].

CS is mucoadhesive (***Table 2***) and this property varies with the degree of acetylation (DA, number of available amine groups): the lower the degree of acetylation, the more free amine groups that will in turn lead to greater mucoadhesive properties, as they become positively charged in low pH environment, enhancing electrostatic interactions with the negatively charged mucins [115, 133].

CS also possesses intrinsic antimicrobial activity, making it a suitable biomaterial for developing new strategies for *H. pylori* infection management [134]. There are several examples in the literature where functionalized CS particles with molecules with bactericidal activity against *H. pylori* effectively reduced the bacterial load [135-137], which also shows the ability of MP and NP to reach the infection site. Moreover, CS has been reported to modulate the activation of immune cells, a property that can vary depending on the presence of contaminants, the degree of purity and its DA [78]. By modulating immune cell phenotypes, such strategies can either enhance tissue regeneration, when lower DA levels are used, or even promote stronger immune stimulation by using CS with a higher DA. A thorough understanding of cellular responses to CS is therefore essential for the development of advanced biomaterial-based strategies [78].

The straightforward functionalization of CS with molecules of interest is possible by its chemical structure (***Figure 7A***) [138]. Its reactive amine and hydroxyl groups allow the addition of several functional groups that may enhance different properties such as solubility, bioavailability, and affinity for target cells, among others [138, 139]. CS can be further modified with norbornene groups, electron-rich alkene groups that are easily excitable, making the polymer highly reactive and enabling a strong bond between norbornene and thiol (-SH) groups in “photoclick” reactions. Norbornene groups can be introduced into CS through a reaction with carbonic anhydride (1:1). The reactive carbonyl groups form a covalent bond with the amine (NH_2) or hydroxyl (OH) groups of

CS, under the acidic conditions necessary to solubilize the CS, along with an organic solvent, such as DMF, to solubilize the carbonic anhydride [140] (***Figure 7***).

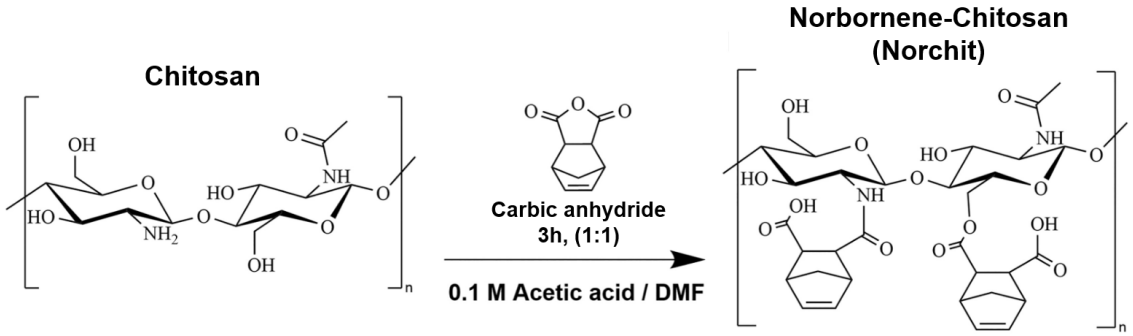


Figure 7. **Norbornene groups conjugation onto chitosan** after reaction with carbonic anhydride in acetic acid/N,N co-solvent system - Dimethylformamide (DMF) to obtain Norbornene modified chitosan (NorChit) as described in [140].

The CS norbornene functionalization and its chemical versatility have been previously described [135, 140, 141]. One of its most interesting features is that this reaction introduces an average of 0.38 norbornene groups per CS monomer, enabling a good yield in the subsequent step for conjugation of the desired bioactive molecules [141]. The production of NorChit-NP can be done by various methods [142], including microfluidics, a fast, reproductible and green technique. In a microfluidic system, the production of NP occurs in microreactors, typically in the form of a chip made from a polymer, such as polydimethylsiloxane (PDMS). Previously, our group developed a system that allows to obtain and functionalize NP in a single step ("one-pot") with high reproducibility [135]. Briefly, within a continuous laminar flow system, two controlled interruptions occur due to the sequential mixing of new solutions (***Figure 8***). The first interruption introduces Type I water into the NorChit stream, enabling the formation of the NP core that then passes through a serpentine channel to stabilize. The second interruption introduces the molecule to be grafted, which binds to the surface of the previously formed NP. This step is also followed by a serpentine channel to ensure proper stabilization [143].

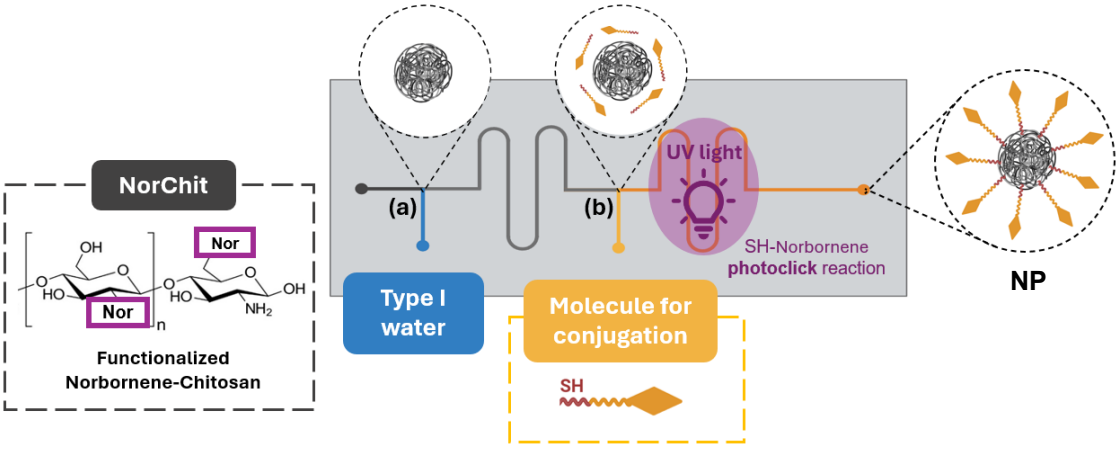


Figure 8. **Schematic representation of nanoparticle (NP) production in a microfluidic system using NorChit and thiolated molecule for conjugation.** In a microfluidic system, NP are formed in **(a)** through intersection of the functionalized norbornene chitosan (NorChit) with Type I water and stabilized in the subsequent coil. In **(b)**, the molecule of interest containing a thiol (-SH) group is introduced together with a photoinitiator and grafted onto the previously formed NP through a "photoclick" reaction enabled by ultraviolet (UV) radiation. Functionalized NP are then stabilized in the subsequent coil. Image not to scale and created with *Biorender.com*.

The grafting of the molecule of interest can be achieved through "photoclick" chemistry, provided that the molecule is thiolated (-SH) and prepared in a solution containing a photoinitiator [135]. A photoinitiator is a compound that, upon exposure to ultraviolet (UV) light, generates reactive species (typically free radicals) capable of initiating the crosslinking reaction [144]. "Photoclick" chemistry is a selective bioconjugation approach that enables the formation of thiol-ene bonds under UV irradiation [145]. "Photoclick" chemistry stands out from others, such as the Copper-Catalyzed Azide-Alkyne Cycloaddition (CuAAC), or Strain-Promoted Azide-Alkyne Cycloadditions (SPAAC) [146], due to its speed, its efficiency of grafting (high yield reaction) and ease of execution [141].

II. Aim

The development of cholesterol-functionalized nanoparticles (NP) as an innovative strategy for the control of *Helicobacter pylori* (*H. pylori*) infection is particularly appealing, as this gastric pathogen relies on this molecule for survival [65]. Previous proof-of-concept studies used gold NP functionalized with cholesterol to demonstrate their specific antimicrobial potential [74]. Building on these findings, norbornene-modified chitosan nanoparticles functionalized with cholesterol (Chol-NP) were subsequently developed, since chitosan is a biocompatible polymer suitable for “real world” translation.

In this work, the biological safety profile of Chol-NP is depicted, including its cytocompatibility and hemocompatibility. Furthermore, as the immune system is strongly activated during *H. pylori* infection, leading to a chronic sustained inflammation, investigating whether Chol-NP have an impact on immune cells, in specific on macrophages, is a critical step to further support the development of these NP as a novel therapeutic approach for the treatment of *H. pylori* infection.

To achieve this, the following specific objectives were defined:

1. Produce Chol-NP and control NP (composed solely of NorChit, without cholesterol functionalization; NC-NP) using a microfluidic system;
2. NP (Chol-NP and NC-NP) characterization, namely concentration (NP/mL) and hydrodynamic diameter (nm) using Nanoparticle Tracking Analysis (NTA);
3. Assess cytocompatibility of the NP (Chol-NP and NC-NP) through metabolic activity assays with resazurin in AGS (ATCC® CRL-1739) and MKN28 (ATCC® CRL-2947) gastric cell lines;
4. Determine the Chol-NP and NC-NP hemocompatibility;
5. Assess cytocompatibility of the NP (Chol-NP and NC-NP) on human macrophages using metabolic activity assays and evaluate cellular polarization by quantifying surface markers (CD86, CD40, HLA-DR, CD163, and CD206) using flow cytometry.

III. Material and Methods

1. Microfluidic system

The microfluidic system used for the nanoparticles (NP) production was designed as described elsewhere [135]. Briefly, the mold for the microfluidic system was done using OpenSCAD software (version 2019.05). The main channel was defined as 36.5 mm, and the side channels were 5 mm long. Both the width and depth of all channels were set to 200 µm and 80 µm, respectively. The serpentine region of the microfluidic chip had a footprint of 5.5 mm × 8 mm, corresponding to the width and length of the structure in top view, as illustrated in ***Figure 9***. The molds were printed using a Form 3 stereolithography printer (Formlabs; 25 µm resolution), after confirming the feasibility of the design. Clear resin (Clear Resin V4; Formlabs) was used for printing. Following fabrication, the molds underwent post-processing consisting of two 15 minutes immersions in isopropanol (Enzymatic, SA) to remove any uncured resin. The drying step was performed by thermal treatment at 80 °C overnight.

A mixture of polydimethylsiloxane (PDMS) and curing agent in a 9:1 ratio (Sylgard™ 184, Elastomer Kit) was poured over the mold of the system (≈ 3 mL of solution) and subsequently cured at 70°C for 2 hours. After curing, the microfluidic circuits were peeled off from the mold, and outlet ports were created using a 1 mm biopsy punch (KAI Medical, BP-50F). To clean the mold for reuse, low-residue adhesive tape (3M 471 Tape, 50 mm × 33 m; Rodrigues & Boaventura, LDA) was applied.

Finally, one side of the PDMS device was irreversibly bonded to a clean glass slide (previously cleaned with 70% v/v ethanol, Sigma-Aldrich) using oxygen plasma treatment (Tergeo Plasma Cleaner, Pie Scientific (TG100)). This final step helps to prevent leakages from the microfluidic system.

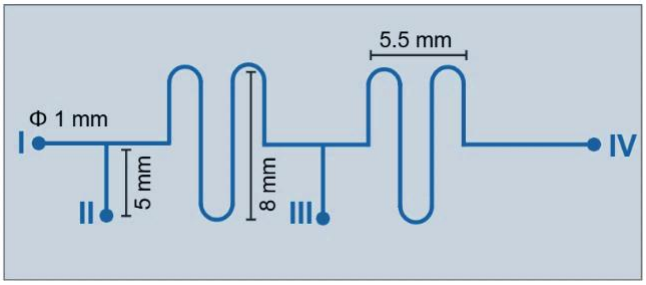


***Figure 9*. Schematic representation of the designed microfluidic system** with respective channel dimensions and diameter of the inlets (I, II, III and IV). Image created using *Biorender.com* (not to scale).

2. Norbornene-modified chitosan (NorChit)

The norbornene-modified chitosan (NorChit), used as the core material for the nanoparticles (NP), was prepared according to the method described in [140]. Briefly, purified squid-derived chitosan (France Chitine), with a degree of acetylation (DA) of 2–3% (confirmed by ^{1}H NMR and FTIR) and a molecular weight (MW) of 363 ± 28 kDa [135], was dissolved overnight in 0.1 M acetic acid (AppliChem) to a final concentration of 0.4% w/v.

Norbornene groups were introduced onto chitosan via reaction with carbic anhydride in *N, N*-dimethylformamide (DMF; 0.15 M, Merck), added every 30 minutes for a total of three additions. The reaction was allowed to proceed for 3 hours at Room Temperature (RT; 22°C). The resulting solution was dialyzed to remove residual solvents using a 10 kDa molecular weight cutoff membrane (Thermo Scientific SnakeSkin), against decreasing concentrations of sodium chloride (NaCl; VWR Chemicals) in Type II water (purified water with resistivity > 1 MΩ·cm, conductivity < 1 µS/cm, and total organic carbon < 50 ppb), over a period of 4 days. Dialysis was carried out at 40°C for the first 48 hours, with buffer replacement three times daily.

Afterwards, the NorChit polymer was frozen (-20°C), lyophilized at -50°C (LABCON), and stored at -20°C under a nitrogen atmosphere until further use.

3. Norbornene chitosan nanoparticles (NC-NP) and Cholesterol nanoparticles (Chol-NP) production

The NorChit solution (1.5 mg/mL), was hydrated in Type I water (ultrapure water with resistivity >18 MΩ cm, conductivity <0.056 µS/cm, and total organic carbon <50 ppb; Merck Millipore) one day prior to its use. Hydration was performed under gentle agitation at 4°C, over 8 hours. Afterwards, glacial acetic acid (0.1 M; AppliChem Panreac) was added to completely dissolve the polymer, and the solution was left overnight under the same conditions.

The cholesterol solution to be injected in the microfluidics (Chol, 2 mg/mL) was prepared immediately before use, using two solutions: (i) a stock solution (30 mg/mL) of Cholesterol-PEG_{75}-Thiol (75 polyethylene glycol (PEG) repeats; MW 3400 Da; Nanocs, PG2-CSTH-3k) previously dissolved in absolute ethanol (Sigma-Aldrich) and; (ii) stock solution (4 mg/mL) of the photoinitiator VA-086 (4%; Fujifilm (Global)) prepared in phosphate buffer (0.2 M $H_2NaO_4P{\cdot}H_2O$ and 0.2 M HNa_2O_4P; Sigma-Aldrich). After

preparation, the stock solutions were mixed in phosphate buffer. Specifically, 6.6% (v/v) of solution (i), 10% (ii) and 83.4% v/v of phosphate buffer to obtain the final working solution (Chol, 2 mg/mL).

The different solutions (NorChit, Type I water and Chol) were injected into the microfluidic system through the corresponding inlets at defined flow rates, as outlined in ***Figure 10***, using syringe pumps (New Era).

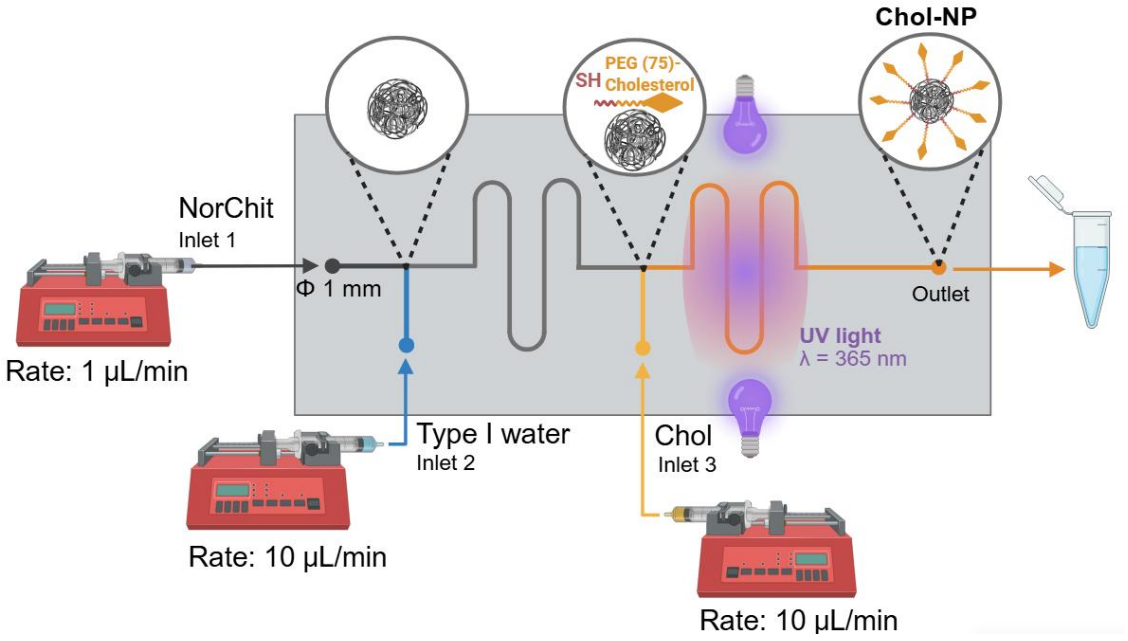


Figure 10. **Schematic representation of the production of Cholesterol Nanoparticles (Chol-NP)** using a microfluidic system. Image created using *Biorender.com* (not to scale).

The NorChit solution, injected through the first inlet, intersects the Type I water solution introduced into the second inlet, resulting in the formation of Norbornene chitosan nanoparticles (NC-NP), as illustrated in ***Figure 10***. Subsequently, in the third inlet, the Chol solution intersects the flow in the presence of two parallel ultraviolet-LED (UV-LED) light sources (λ = 365 nm, Mouser Electronics Inc.; distance from the microfluidic system: top LED ~4 cm, bottom LED ~0.5 cm; intensity: top LED 35 mW/cm², bottom LED 75 mW/cm²; combined light intensity on the NP: 110 mW/cm²). This exposure promotes a "photoclick" reaction between the -SH group of the Chol molecule and the norbornene groups on the NC-NP. The resulting Chol-NP were collected at the outlet (***Figure 10***) and filtered using Amicon filters (50 kDa, Sigma-Aldrich) by centrifugation (1700 *g*, RT, 10 minutes; Eppendorf® 5810 R). The NP retained on the filter was subsequently resuspended in Type I ultrapure water. The same procedure was done for obtaining non functionalized NP (NC-NP), by only injecting Type I water into the third inlet (instead of the Chol solution).

To ensure optimal sterility prior to the NP preparation, the working bench was thoroughly disinfected using 70% v/v ethanol (VWR), and the NP were collected in sterile microcentrifuge tubes, which were immediately closed and sealed with Parafilm (Frilabo). To confirm the NP sterility, 20 µL of each NP batch was inoculated onto Tryptic Soy Agar (TSA; Sigma-Aldrich) plates, followed by incubation for 24 hours at 37°C. TSA was the culture media chosen because of its broad ability to support the growth of a wide variety of bacteria and fungi.

4. Nanoparticle characterization

The obtained NP (Chol-NP and NC-NP) were characterized in terms of concentration and hydrodynamic diameter. Both parameters were measured using a NanoSight NS300 instrument (NTA Dev Build 3.2.16) equipped with an sCMOS camera (Malvern Instruments). Prior to analysis, the samples were diluted in Type I water to obtain working concentrations within the range of 10^8 NP/mL. Three 30 seconds videos were recorded for each sample (with a limit of 10 to 50 particles per frame). Data acquisition and processing were performed using the NanoSight NS300 NTA 3.0 software.

5. Nanoparticles cytotoxicity studies

5.1 Cell lines

5.1.1 Culture

Two gastric cell lines were used: the human gastric adenocarcinoma AGS cells (ATCC® CRL-1739), derived from a human gastric adenocarcinoma and recognized for their strong acid-secretory function, and the MKN28 cell line (ATCC® CRL-2947), which exhibit better-preserved cell polarity and certain morphological features of intestinal epithelium. Cells were cultured in Roswell Park Memorial Institute medium (RPMI; Gibco) supplemented with 10% v/v heat-inactivated fetal bovine serum (FBS; Biowest; heat inactivated at 56°C for 30 minutes) and 1% v/v penicillin/streptomycin (Pen/Strep; Biowest), herein referred to as complete RPMI. Cultures were maintained at 37°C in a humidified atmosphere containing 5% CO_2, until reaching 70-80% confluency.

5.1.2 Metabolic activity assay

After reaching confluency, cells were detached using trypsin (Biowest) at 37°C and 5% CO_2 for 5 minutes and seeded at a density of 1×10^4 cells per well in 96-well plates (SARSTEDT, tissue cultured (TC)-treated suspension plates) for 24 hours at 37°C and in 5% CO_2 for cell viability studies (direct method), following the ISO 10993-5 guideline [74].

Afterwards, NP (Chol-NP and NC-NP) resuspended in complete RPMI were added to the cells. Briefly, the NP suspension was prepared by centrifuging 300 µL of each NP formulation (1700 *g*, RT, 10 minutes; Eppendorf® 5810 R) using Amicon filters (50 kDa, Sigma-Aldrich). The NP trapped on the filter were then resuspended in the same volume of complete RPMI medium, and both the centrifugation and resuspension process were repeated. The centrifugation steps enabled the replacement of the storage solution (Type I water) with culture medium and the removal of any residual solvent that could compromise cell viability. As such, this protocol preserved the concentration of the original NP batch (10^{10} NP/mL) while transferring the NP into a suitable medium for cell culture. Serial dilutions were subsequently prepared to obtain concentrations in the range of 10^9 NP/mL and 10^8 NP/mL, which were added to the wells of the culture plates. Incubation proceeded for 24 hours at 37°C in a humidified 5% CO_2 atmosphere.

After the incubation period, the cell culture medium and the NP were carefully removed, and the wells were washed once with sterile phosphate-buffered saline (PBS; 0.1 M; pH 7.4) to remove any residual NP. Finally, cellular metabolic activity was assessed using a resazurin assay. For this, cells were incubated with a solution of 20% v/v resazurin in complete RPMI medium for 4 hours, 37°C in a humidified 5% CO_2 atmosphere. Additionally, controls for cell growth and cell death were done by including cells not exposed to NP and by treating cells with 2% v/v solution of 30%V H_2O_2 (Merck) in complete RPMI medium, respectively.

Metabolic activity was calculated using the equation (1):

$$(1)\ \%\ Cell\ metabolic\ activity = \frac{Fexp\ - Fblank}{Fcontrol - Fblank}$$

where F_{exp} is the fluorescence of cells exposed to NP, F_{blank} is the fluorescence of complete RPMI medium without cells, and $F_{control}$ is the fluorescence of untreated cells (negative control). Fluorescence measurements were obtained using a microplate

spectrophotometer (SpectraMax iD3; Molecular Devices) with excitation at 530 nm and emission at 590 nm on 96-well Black/Black Bottom plate (Fisher Scientific).

Results were expressed as mean ± standard deviation (SD) and represent four independent experiments with triplicates.

5.2 Macrophages

5.2.1 Isolation of Human Monocytes

Human monocytes were isolated as described in [78] from leukocyte-rich buffy coats obtained from healthy donors, kindly provided by the Department of Immunohematology of the Centro Hospitalar São João (CHSJ), in Porto, Portugal, under the scope of the Ethics Protocol 90/19.

Briefly, buffy coats were first centrifuged at 1200 *g* (speed 5, brake 0; Eppendorf® 5810 R) for 30 minutes at RT. After centrifugation, the peripheral blood mononuclear cells (PBMCs) layer was carefully collected. To enrich for monocytes, 67 µL of RosetteSep™ Human Monocyte Enrichment Cocktail (StemCell Technologies) was added per milliliter of PBMCs. The mixture was then incubated on a horizontal shaker (Stuart) for 20 minutes at RT (speed 17). This enrichment method relies on a negative selection strategy, in which unwanted cells are crosslinked to red blood cells via tetrameric antibody complexes, forming dense immunorosettes. Following incubation, the cell suspension was diluted in PBS supplemented with 2% v/v FBS (Biowest), layered onto Ficoll-Histopaque (Sigma-Aldrich), and centrifuged at 1200 *g* (speed 2, brake 0; Eppendorf® 5810 R) for 30 minutes at RT. During gradient separation, immunorosette complexes, being denser, migrated below the Ficoll layer, while monocytes remained at the interface between the plasma and the density gradient. Afterwards, the monocyte layer was carefully collected, washed three times with PBS (300 *g*, 6 minutes, RT; Eppendorf® 5810 R), and finally resuspended in complete RPMI medium (RPMI (Gibco) supplemented with 10% v/v FBS and 1% penicillin/streptomycin (Pen/Strep) (both from Biowest)). Finally, the cells were counted in a Neubauer chamber using the Trypan Blue dye (Sigma-Aldrich) exclusion method to determine the total number of live cells obtained during isolation.

5.2.2 Cell seeding and metabolic activity assay

Following isolation, monocytes were seeded into 24-well plates (SARSTEDT, TC-treated suspension plates) containing round sterile glass coverslips (Ø 13 mm, VWR) that allowed cell adhesion. Each well received 0.25 × 10^6 cells in complete RPMI supplemented with macrophage colony-stimulating factor (M-CSF) at 50 ng/mL (11343117, ImmunoTools). Cells were incubated for 7 days to allow differentiation into macrophages under standard culture conditions (37°C, 5% CO_2, humidified atmosphere). On day 7, the culture medium was replaced with complete RPMI without M-CSF and the cells were incubated for 10 hours under standard culture conditions. Afterwards, cells were stimulated with Chol-NP or NC-NP (300 µl/well; 10^{10},10^9 and 10^8 NP/mL), following a similar protocol to the one described for the cell lines (section 5.1.2) but with NP incubation time of 72 hours. This extended incubation period was chosen to support the subsequent evaluation of macrophage polarization, since the prolonged exposure to the NP would allow for increased expression and detection of cytokines and cellular markers associated with this process. Macrophages metabolic activity was assessed using the resazurin assay and was calculated as in section 5.1.2 using a Synergy Mx BioTek equipment (λ_{Ex} = 530 nm, λ_{Em} = 590 nm).

6. Nanoparticles hemocompatibility study

Red blood cells (RBCs) were obtained from buffy coats of healthy blood donors that were kindly provided by the Department of Immunohematology of the Centro Hospitalar São João (CHSJ), in Porto, Portugal under the scope of the Protocol 90/19.

The hemocompatibility of Chol-NP and NC-NP was evaluated using a hemolysis assay adapted from [147]. Briefly, RBCs were isolated from the buffy coats by centrifugation (400 *g*, RT, 30 minutes; Eppendorf® 5810 R) using a density gradient with Histopaque-1077 (Sigma-Aldrich). The plasma layer was carefully removed and the collected RBC pellet was washed three times with PBS (370 *g*, RT, 10 minutes per wash; Eppendorf® 5810 R).

The RBCs concentration was standardized to 2 × 10^8 cells/mL in accordance with [74] followed by incubation with Chol-NP or NC-NP at concentrations in the order of magnitude of 10^{10}, 10^9, and 10^8 NP/mL for 3 hours, at 37°C, in round-bottom polypropylene 96-well microplates (Corning). Then, the plate was centrifuged (900 *g*, RT, 10 minutes; Eppendorf® 5810 R) and the supernatant transferred to a flat-bottom 96-well

microplates (Greiner Bio-One) for absorbance reading at 380 nm (A380), 415 nm (A415), and 450 nm (A450) using a microplate spectrophotometer (CLARIOstar® Plus; BMG LABTECH).

The amount of hemoglobin (Hb) was calculated using the following equation (2):

$$(2)\ Hb\ value\ of\ sample\ (mg/dL) = \left[\left(2 \times A415 - (A380 + A450)\right) \times 1000\right]/E$$

Where A415 corresponds to the hemoglobin absorption in the Soret band, while A380 and A450 are correction factors for uroporphyrin, which also absorbs in the same wavelength range. *E* represents the molar absorptivity of oxyhemoglobin at 415 nm, which is 79.46. The hemolytic potential at each tested concentration was then calculated using the following equation (3):

$$(3)\ Hemolysis\ (\%) = \frac{Hb\ value\ of\ sample}{Total\ Hb\ value} \times 100$$

The total hemoglobin value corresponds to 100% hemolysis, induced by 1% v/v Triton X-100 (Sigma Aldrich, X100). Negative controls (containing only RBCs and PBS) were included to ensure that the RBCs were in good physiological condition, and positive controls (1% v/v Triton in PBS) were included to represent 100% hemolysis. All assays were performed in triplicate and repeated three times.

7. Macrophage profile evaluation upon exposure to nanoparticles

For macrophage profile evaluation, only the highest concentration of NP (10^{10} NP/mL) was evaluated. Experimental controls were obtained through stimulation with 10 ng/mL LPS (*Escherichia coli* serotype O55:B5, Sigma-Aldrich), 10 ng/mL of LPS plus 50 ng/mL IFN-γ (11343536 ImmunoTools) and 10 ng/mL of IL-10 (11340105, ImmunoTools), aiming to serve as two pro-inflammatory and one anti-inflammatory controls, respectively, for 72 hours as described in [148].

Following stimulation, macrophages were detached from the coverslips by incubation with Accutase (eBioscience) at 37°C for 30 minutes, followed by gentle scraping with cell scrapers (Sigma-Aldrich). The resulting cell suspension was washed (240 *g*, 4°C, 5 minutes; Eppendorf® 5810 R), and the pellet was resuspended in FACS buffer (PBS, 2% v/v FBS (Biowest) and 0.01% v/v sodium azide (Sigma-Aldrich)). The suspension was then transferred to a round-bottom polypropylene 96-well microplates (Corning) for

staining. For that, the cells were washed with FACS buffer and immunolabeled in the dark for 45 minutes at 4°C with the following antibodies: anti-human CD14-APC (1:50; 21279146X2, ImmunoTools), CD86-FITC (1:50; 21480863X2, ImmunoTools), HLA-DR-FITC (1:200; 48-9952-42, Invitrogen), CD40-FITC (1:50; 21270403, ImmunoTools), CD163-PE (1:9; 556018, BD Pharmingen™) and CD206-PE (1:200; 321106, BioLegend) and with Live Dead (LD, viability dye eFluor™) (1:10000; 780 - 65-0865-14, Invitrogen) solution diluted in PBS. After staining, cells were washed three times with FACS Buffer (240 *g*, 4ºC, 5 minutes; Eppendorf® 5810 R) and then fixed in 2% v/v paraformaldehyde (PFA; Sigma-Aldrich) for 15 minutes, in the dark and at 4ºC. Finally, the cells were centrifuged (240 *g*, 5 min, 4°C; Eppendorf® 5810 R) and resuspended in 200 µL of FACS buffer. The plate was stored at 4°C until further analysis on the cytometer.

Unstained cells (US) and single-stained samples were also included. For single-stained controls, compensation beads (Invitrogen, 01-2222-42) were used. Briefly, one drop of beads was dispensed into a microcentrifuge tube for each antibody, followed by centrifugation (600 *g*, 5 min, 4°C; Eppendorf® 5810 R). The supernatant was discarded, and the pellet was carefully resuspended in 50 µL of the corresponding antibody solution (maintaining the staining dilutions). The mixture was incubated for 30 minutes at 4°C, protected from light. Afterwards, the beads were washed twice with FACS buffer, centrifuged at 240 *g* for 5 min at 4°C and were then resuspended in 200 µL of FACS buffer and kept at 4°C until further analysis.

Prior to analysis, samples were filtered through a 100 µm nylon mesh (Sigma-Aldrich) and data were acquired on a FACS Canto Flow Cytometer (BD Biosciences) using BD FACSDiva™ software. Data was analyzed using FlowJo software (v10.7.2).

The gating strategy is shown in ***Figure 11***. Following live cell-gating, the percentage of positive cells for CD14, CD86, CD40, HLA-DR CD163 and CD206, together with their expression levels quantified as median fluorescence intensity (MFI), were determined through the removal of the unstained sample (US) controls.

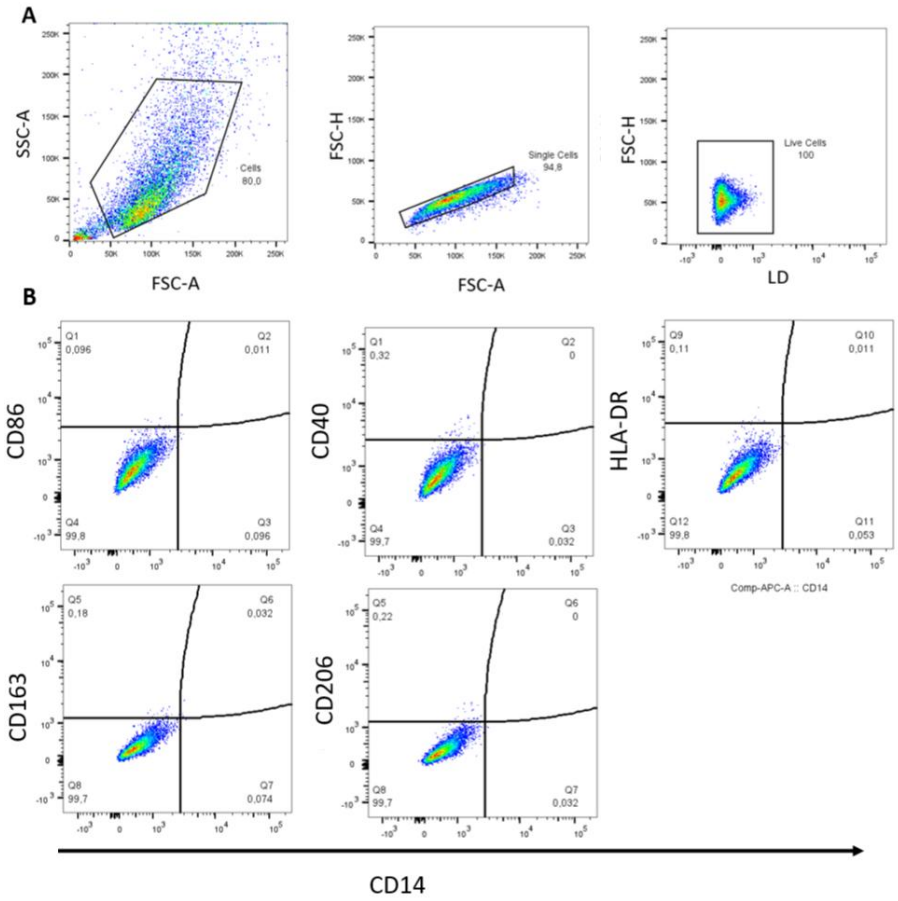


Figure 11. **A) Gating strategy to evaluate macrophage polarization**. Monocytes were isolated from the buffy coat of healthy donors by negative selection using the Monocyte Enrichment Kit (RosetteSep). **B) Polarization profile of monocytes** was assessed by analyzing the expression of CD14 (a macrophage lineage marker), CD86, CD40, HLA-DR, CD163 and CD206 after 72 hours of stimulation. The example shown corresponds to the unstained sample (US). *FSC - forward scatter, SSC - side scatter, LD - Live death*

8. Statistical analysis

Graphics and statistical analyses were performed using GraphPad Prism software (GraphPad Software Inc., version 8.0). For the cytotoxicity assays in gastric cancer cell lines (AGS and MKN28), Ordinary one-way ANOVA was applied. For macrophage cytotoxicity assays, unpaired t-test was used, and when the assumption of equal variances was not met, Welch's correction was applied to account for unequal standard deviations between groups. For flow cytometry data and for the hemolysis assays, due to the limited number of biological donors (n <7), a non-Gaussian distribution was assumed, and the nonparametric Friedman test was used for pairwise comparisons between experimental conditions. Differences were considered statistically significant at $*$ or # $p < 0.05$, $**p < 0.01$, and $***p < 0.001$.

IV. Results and Discussion

1. Nanoparticles (NP) characterization

The nanoparticles (NP) produced, Cholesterol-functionalized norbornene chitosan nanoparticles (Chol-NP) and norbornene chitosan nanoparticles (NC-NP) were characterized in Type I water regarding their size (hydrodynamic diameter, expressed in nm) and concentration, expressed as the number of particles per milliliter (NP/mL) using the Nanoparticle Tracking Analysis (NTA) technique. Results are summarized in ***Table 3***.

Table 3. **Nanoparticle characterization** (hydrodynamic diameter, D10, D50, D90, and concentration) was performed by Nanoparticle Tracking Analysis (NTA). D10, D50, and D90 represent the diameters below which 10%, 50%, and 90% of the particle population are found, respectively. Data are expressed as mean ± standard deviation (SD), n = 3.

NP	Hydrodynamic diameter (nm)	D10 (nm)	D50 (nm)	D90 (nm)	Concentration 10^{10} (NP/mL)
Chol-NP	163.9 ± 35.8	107.4 ± 32.4	167.3 ± 31.4	229.5 ± 60.1	1.5 ± 1.4
NC-NP	116.7 ± 7.1	85.8 ± 13.4	103.9 ± 10.6	166.9 ± 7.2	2.1 ± 1.4

Quantification of particle concentration was essential to ensure experimental reproducibility on the subsequent biological assays, which were performed using NP from different batch productions. In parallel, the evaluation of NP size (hydrodynamic diameter) aimed to confirm batch-to-batch consistency and to ensure that NP size remained above 100 nm, thereby reducing the risk of unintended translocation across cellular barriers [149].

Chol-NP had an average size of 163.9 ± 35.8 nm (***Table 3***) slightly larger than the control NC-NP, that had an average diameter of 116.7 ± 7.1 nm. This increase in size is consistent with what would be expected following the cholesterol functionalization, since the presence of this hydrophobic moiety can promote changes in NP packing and surface organization, resulting in an increased hydrodynamic diameter [150]. It is worth noting that although the Chol-NP had higher size variability, reflected by a larger standard deviation, the D50 value is close to the mean hydrodynamic diameter, which generally means that the size distribution is narrow and symmetrical, indicating that there are no large outliers disproportionately influencing the mean. Therefore, the Chol-NP sample is likely slightly polydisperse, with most particles clustered around the same size range. NC-NP had a narrower size distribution (D10 = 85.8 nm; D90 = 166.9 nm), consistent with their lower variability. The size of NC-NP was comparable to that reported in a

previous study (107 ± 55 nm), although the herein obtained concentration was approximately ten times lower than the one reported in the literature (2.2 ± 0.2 × (10^{11} NP/mL)) [135]. Several hypotheses may account for this: one possibility relates to differences in the microfluidic system configuration, which can depend on the operator's technique as well as on the specific equipment used (e.g., pumps and syringes). Another factor could be variations attributed to the NP quantification by NTA technique, as this method is sensitive to parameter settings and operator-dependent adjustments. Regarding Chol-NP, a concentration of (1.5 ± 1.4) × 10^{10} NP/mL was obtained. Although particles with directly comparable characteristics were not found in the literature, the concentration obtained remained in the same order of magnitude as the one of the non-functionalized particles.

In addition, the successful grafting of cholesterol-PEG-SH (Chol) onto the NorChit-NP (NC-NP) backbone has been confirmed by our group by Attenuated Total Reflection – Fourier Transform Infrared Spectroscopy (ATR-FTIR) analysis [151].

2. Cyto- and hemocompatibility of Cholesterol nanoparticles (Chol-NP) and NorChit nanoparticles (NC-NP)

2.1 Cytocompatibility in Gastric Cell lines

The cytotoxicity of Chol-NP and NC-NP was evaluated in two gastric cell lines: AGS (ATCC® CRL-1739) and MKN28 (ATCC® CRL-2947). Both lines are widely used as *in vitro* models in gastric cancer research, as while they are both derived from human gastric adenocarcinomas, they exhibit distinct phenotypes [152]. AGS cells originate from a primary gastric adenocarcinoma and display a moderately differentiated gastric epithelial phenotype [153]. In contrast, MKN28 cells are derived from well differentiated gastric adenocarcinoma and present an intestinal phenotype [154]. These two cell lines thus represent complementary models for evaluating the biocompatibility of NP based systems with potential applications in the gastrointestinal context [155, 156]. Throughout the assays, no alterations in cell morphology or confluence were observed. AGS cells exposed to NP retained their characteristic epithelial phenotype, displaying polygonal shapes and monolayer growth comparable to the untreated control, as described in [74]. Likewise, MKN28 cells maintained their flattened morphology with visible cytoplasmic extensions, a tendency to form clusters, and organized monolayer growth [135].

Cytotoxicity assays (direct assays) were conducted in accordance with the ISO standard 10993-5 [74] and results are shown in ***Figure 12***.

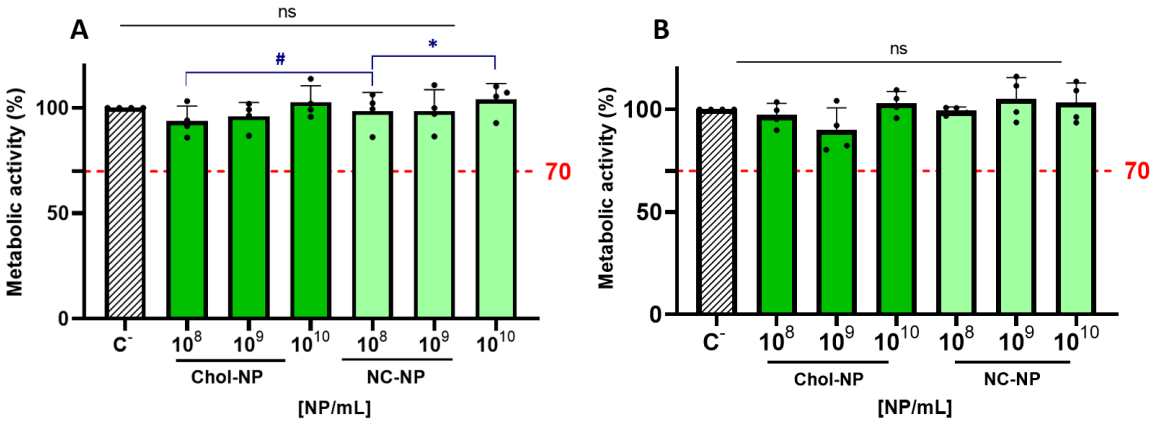


Figure 12. **Metabolic activity of A) AGS, and B) MKN28 cell lines** exposed to Cholesterol nanoparticles (Chol-NP) and NorChit nanoparticles (NC-NP) at increasing concentrations (10^8, 10^9, and 10^{10} NP/mL), normalized to the negative control C^- (untreated cells). The positive control (not shown) consisted of cells incubated with a 2% v/v solution of 30% V H_2O_2. Cells metabolic activity was assessed by the resazurin assay (n = 4, with triplicates), and data are presented as mean ± SD. Statistical analysis was performed using an Ordinary one-way ANOVA, and no statistically significant difference (ns) was observed between the different conditions and negative control (C^-). * $p < 0.05$ between the lowest concentration (10^8 NP/mL) and the highest concentration (10^{10} NP/mL) of NC-NP; # $p < 0.05$, between Chol-NP and NC-NP at 10^8 NP/mL. The dotted red line corresponds to the 70% threshold of cytotoxicity according to ISO 10993-5 [74].

The results (***Figure 12***) demonstrate that neither type of NP (Chol-NP or NC-NP), at any of the concentrations tested (10^{10}, 10^9, and 10^8 NP/mL), significantly altered the cells metabolic activity when compared to the untreated control (C^-, ***Figure 12***), indicating that no cytotoxic effect was seen on these cell lines. Since NorChit is chitosan (CS) functionalized with norbornene groups, it likely conserves the key characteristics of CS, such as biocompatibility [138], being these results consistent with the properties of reported in the literature.

In AGS cell line a statistically significant difference was observed between Chol-NP at the concentration of 10^8 NP/mL and Chol-NP at the highest concentration, 10^{10} NP/mL (*p <0.05), with metabolic activity increasing as the Chol-NP concentration increased. This indicates that cells increase their metabolic activity under these conditions, where NP may be promoting cell viability. Regarding the analysis of the two different types of NP (Chol-NP and NC-NP) at the same concentration (10^8 NP/mL), statistically significant differences (#p < 0.05) were observed between NC-NP and Chol-NP at the same concentration, demonstrating lower metabolic activity in AGS cells treated with Chol-NP. The observed reduction in metabolic activity of AGS cells following NP exposure may be due to several mechanisms: NP are known to interact with cellular membranes and

organelles, potentially impairing mitochondrial function, reducing ATP production, and thereby suppressing metabolic activity [157, 158]. However, although there is reduction of metabolic activity, it is still above the 70% threshold in accordance with the ISO standard [74] to be considered as cytotoxic effect. Therefore, complementary assays assessing cell viability, apoptosis, oxidative stress markers, and mitochondrial membrane potential would be interesting to further clarify if the reported changes reflect true biological changes following NP exposure. For the MKN28 cell line, no statistically significant differences were observed for Chol-NP and control NP (NC-NP) at the same concentration nor between different concentrations for the same NP formulation.

2.2 Hemocompatibility in Reb Blood Cells (RBCs)

The hemolytic profile of Chol-NP and NC-NP was assessed using a hemolysis assay on human red blood cells (RBCs). This test is essential for biomaterials intended for use in gastric infections caused by *H. pylori*, due to the presence of hemorrhagic ulcers at the infection site [159]. Furthermore, these ulcers provide a direct entry route into the bloodstream, reinforcing the importance of evaluating the biocompatibility and interaction of the NP with cellular components of blood. As shown in ***Figure 13***, the *in vitro* hemolysis values after exposure to the designed NP were below the 2% threshold established by the ASTM E2524-08 [160], therefore showing that these NP are non-hemolytic.

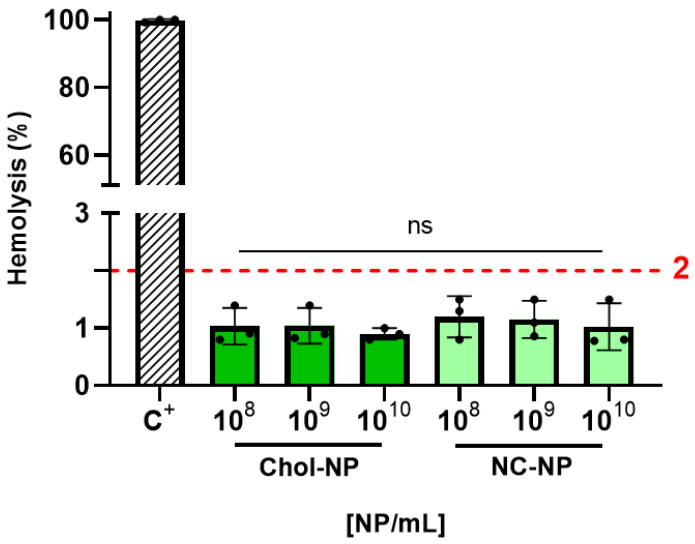


Figure 13. **Hemolysis assay.** Hemolysis percentage (%) determined by hemoglobin release after incubation with Cholesterol nanoparticles (Chol-NP) and NorChit nanoparticles (NC-NP) at different concentrations (10^8, 10^9, and 10^{10} NP/mL), normalized to the positive lysis control C^+ (1% Triton X-100 in PBS). Data are presented as mean ± SD (n = 3, with triplicates). Statistical analysis was performed using a Friedman test and non-statistically significant (ns) differences were observed between Chol-NP and NC-NP. The dotted red line represents the 2% threshold accepted by the ASTM E2524-08 as non-hemolytic [160].

2.3 Cytocompatibility in Human Macrophages

Macrophages were chosen as a cellular model due to their central role in orchestrating the immune response, participating in the recognition and phagocytosis of pathogens, the regulation of inflammation through cytokine release, and the polarization into distinct phenotypes (M1/M2), influenced by environmental conditions or interactions with biomaterials, such as NP [85].

Before performing flow cytometry assays to assess macrophage polarization status, the metabolic activity of human macrophages after exposure to NP was evaluated using the resazurin reduction assay. Assessing cytotoxicity beforehand allowed the selection of NP concentrations that maintained adequate cell viability to perform further assays, thereby ensuring that changes detected in flow cytometry were attributable to immunomodulatory effects rather than to non-specific cell death or metabolic impairment.

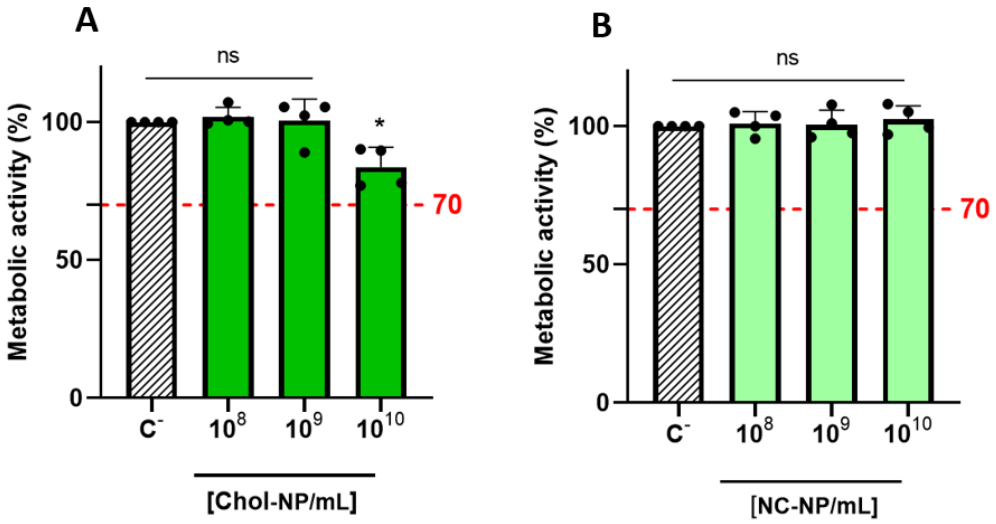


Figure 14. **Metabolic activity of human macrophages** exposed to increasing concentrations (10^8, 10^9 and 10^{10} NP/mL) of **A**) Cholesterol nanoparticles (Chol-NP), **B**) NorChit nanoparticles (NC-NP) and normalized to the negative control C^- (untreated cells). Metabolic activity was assessed by the resazurin assay (n = 4, with triplicates) and data are presented as mean ± SD. Statistical analysis was performed using an unpaired *t*-test, and differences were considered not statistically significant (ns) or statistically significant to C^- at $*p< 0.05$. The dotted red line represents the 70% threshold cytotoxicity according to ISO 10993-5 [74].

Following 72 hours of exposure to the Chol-NP, the 10^8 and 10^9 NP/mL concentrations showed no effect on the macrophages metabolism, whereas at the highest concentration tested (10^{10} NP/mL) a reduction of approximately 16% was observed relative to the control (***Figure 14A***). Nevertheless, since metabolic activity remained above the 70% threshold, the 10^{10} NP/mL concentration was considered suitable to proceed to the flow cytometry assays. NC-NP did not impact macrophage metabolic activity at any of the tested concentrations, with values remaining comparable to the control (untreated macrophages) (***Figure 14B***).

As depicted in ***Figure 15***, macrophages incubated with Chol-NP (***Figure 15B***), showed a more elongated phenotype, a significant morphological change when compared to untreated cells (macrophages without exposure to NP) (***Figure 15A***).

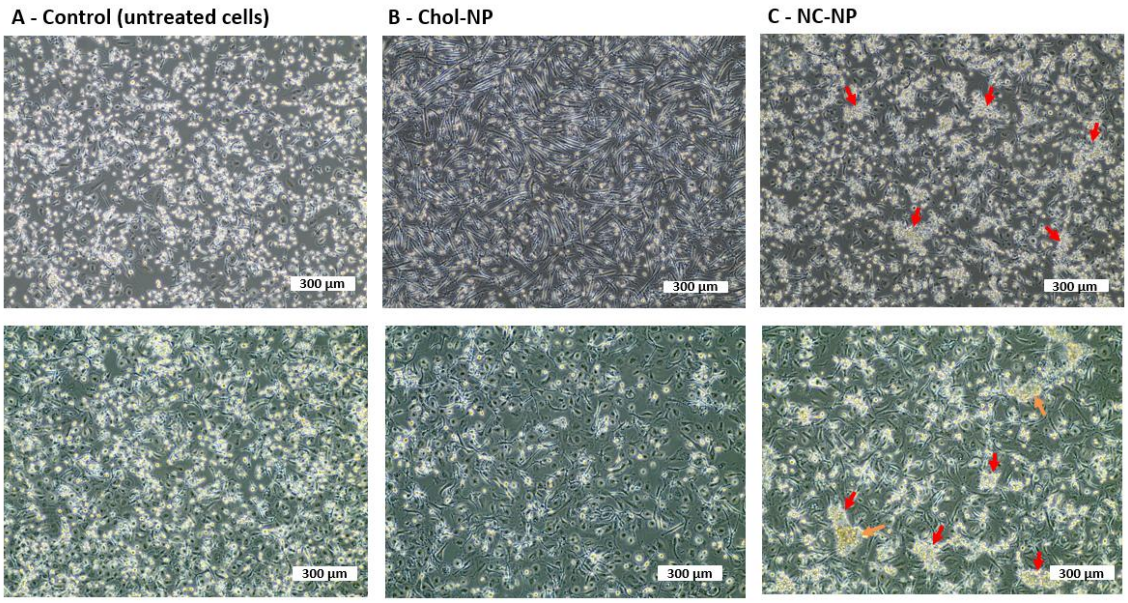


Figure 15. **Phenotype of macrophages A) before and, B) after being stimulated with Cholesterol nanoparticles (Chol-NP) or C) with NorChit nanoparticles (NC-NP) at NP concentrations in the order of magnitude of 10^{10} NP/mL. A)** Unstimulated macrophages exhibiting typical morphology. **B)** Macrophages treated with Chol-NP display an elongated morphology and pronounced cellular alterations. **C)** Macrophages incubated with NC-NP maintained similar morphology to the control (15A), although an increase in aggregated cellular debris (indicated by red arrows) is observed, in addition to floating dead cells (indicated by orange arrows). The **upper panels** correspond to Assay I, and the **lower panels** to Assay II (independent assays). Images were acquired at 10x magnification (bright field).

Cell elongation in macrophages has been described in the literature as associated with cytoskeletal reorganization processes, which may enable cellular interactions with the NP [161]. Furthermore, this phenomenon may reflect changes in activation state [162], as more elongated morphologies have often been associated with the M1 (pro-inflammatory) phenotype as previously reported by our team [162]. Nevertheless, this morphological change alone does not allow to confirm polarization as further validation through flow cytometry analyses is required.

Cells exposed to the NC-NP (***Figure 15C)*** maintained a similar morphology to the control (untreated macrophages) (***Figure 15A***), although there was an increase in cellular debris, which appeared in clusters (***Figure 15C,* red arrows**). Cellular debris is naturally present in cell culture, consisting of remnants from dead or apoptotic cells, and is found in any assay due to the physiological turnover of the cell population [163]. Nevertheless, the formation of debris aggregates, observed specifically in macrophages treated with NC-NP (***Figure 15C***), can be explained by the cationic nature of Chitosan [135]. The Chitosan positive charge enables electrostatic interactions with negatively charged cellular remnants, such as phosphate groups in membrane phospholipids [164], further promoting the aggregation of debris and/or dead cells floating in the medium.

3. Macrophage profile evaluation

To assess if Chol-NP and NC-NP impact the polarization of human macrophages, the expression of surface markers characteristic of specific polarization phenotypes was evaluated, along with the lineage marker CD14. Specifically, CD86, CD40, and HLA-DR were selected as markers associated with the pro-inflammatory M1-like phenotype [83], as their upregulation reflects enhanced antigen-presenting capacity and co-stimulatory activity [165, 166]. Conversely, CD163 and CD206 were analyzed as representative markers of the anti-inflammatory M2-like phenotype, which are typically involved in tissue remodeling, clearance of cellular debris, and resolution of inflammation. The chosen panel is widely validated in the literature for distinguishing functional polarization states in human macrophages [167].

In addition, cell viability was controlled by excluding $CD14^+$ cells that stained with the viability dye (LD). Since this dye penetrates cells with compromised membrane integrity, it allows the identification and exclusion of non-viable cells, ensuring that marker expression was analyzed only in live macrophages. ***Figure 16*** shows the percentage of viable $CD14^+$ cells obtained from an assay performed with three healthy human donors.

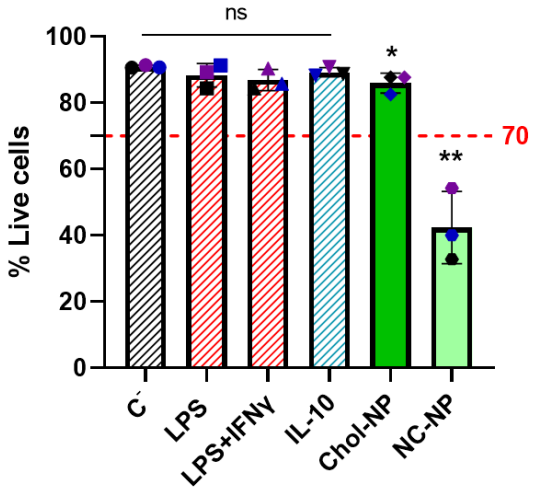


Figure 16. **Effect of Cholesterol-nanoparticles (Chol-NP) and NorChit-nanoparticles (NC-NP) on human macrophages polarization** (n = 3). "C–" corresponds to the negative control (untreated cells). Lipopolysaccharide (LPS) was used as a positive control for bacterial infection, whereas LPS + interferon-gamma (IFN-γ) served as a positive control for bacterial infection in an inflammatory environment. Interleukin-10 (IL-10) was used as positive control for an anti-inflammatory environment. Statistical analysis was performed using the Friedman test, with all comparisons made against untreated control. Differences were considered statistically significant at $*p < 0.05$, $**p < 0.01$ or not significant (ns). Dotted red line shows the 70% threshold regarding cytotoxicity according to ISO 10993-5 [74].

Looking at the % of live cells exposed to the two types of NP, NC-NP had a marked reduction in cell viability (below the ISO 10993-5 70% threshold) (***Figure 16***). Due to experimental constraints, the NP concentration was only determined after macrophage

stimulation, and therefore the concentration could not be normalized beforehand. Therefore, this cytotoxic profile might be linked to the fact that the NC-NP concentration used was five-fold higher (5.56×10^{10} NP/mL) compared to the concentrations used in other assays (***Table 3***). Reinforcing this is also the fact that the prior metabolic activity assays performed and described in Section 2.3 (***Figure 14***) did not reveal cytotoxicity for this type of NP (n = 4) within the usual concentration range (***Table 3***). In contrast to the NC-NP, the concentration obtained for the Chol-NP batch (1.41×10^{10} NP/mL) was comparable to those of previous batches previously used and no reduction in the overall cell viability was observed, being consistent with previous results (***Figure 14*** vs ***Figure 16***).

Regarding the expression of surface markers, levels were evaluated after stimulation only with Chol-NP. Due to the decreased viability of cells treated with NC-NP (***Figure 16***), the results for this condition were not considered to be discussed, as it is not possible to determine whether the changes in marker expression result from immunomodulatory mechanisms or from cell death. In addition to NP stimulation, staining in positive controls for different polarization phenotypes was analyzed. For the M1 polarization profile, the positive controls were i) stimulation with lipopolysaccharide (LPS), simulating a bacterial infection, and ii) LPS plus interferon-gamma (IFN-γ), simulating a bacterial infection combined with an inflammatory environment. For the M2 profile, the positive control was stimulated with interleukin-10 (IL-10).

3.1 Evaluation of the expression profile of CD163 and CD206

The scatter plots presented in ***Figure 17A*** and 17***B*** show the distribution of surface marker expression in a representative experiment, illustrating the differences in the expression of CD163 (scavenger receptor) and CD206 (mannose receptor), both associated with the M2 phenotype, in the various stimulation conditions reported in ***Figure 16***. From these plots, it was possible to select double-positive cells ($CD14^+CD163^+$ or $CD14^+CD206^+$) in each experimental condition, as demonstrated in ***Figure 17C*** and 17***D***.

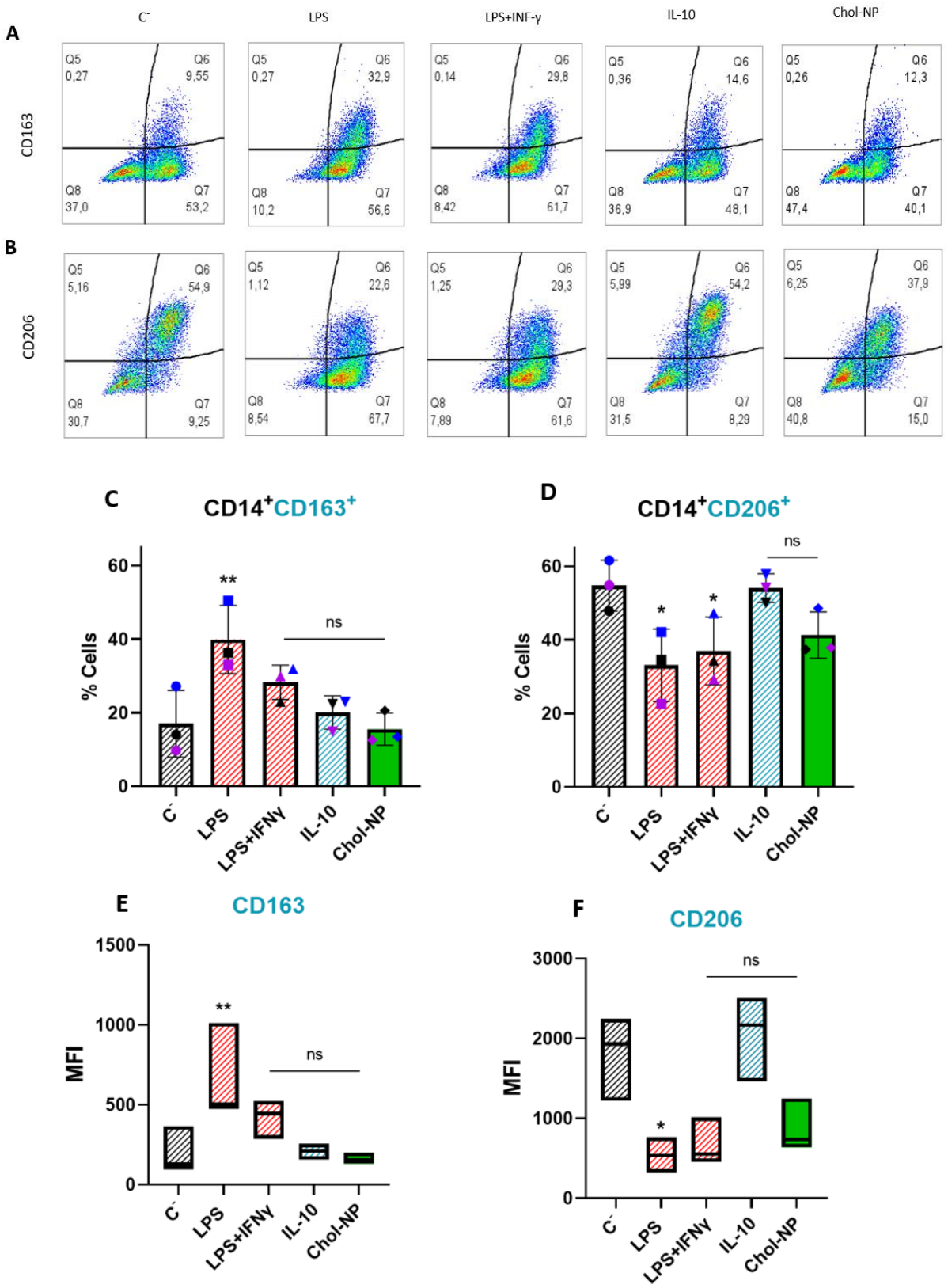


Figure 17. **Surface marker expression is presented as scatter plots for A) CD163 and B) CD206, and the corresponding percentage of positive cells (% Cells) in C) and D), from human macrophages** (n = 3) differentiated in the presence of M-CSF for 7 days. Cells were subsequently cultured for 72 hours with Chol-NP, LPS (lipopolysaccharide; M1), LPS + INF-γ (LPS + interferon-gamma; M1), or IL-10 (M2), "C⁻" corresponds to the negative

control (untreated cells). **Median fluorescence intensity (MFI) of E) CD163 and F) CD206** was calculated by subtracting the fluorescence intensity of the corresponding unstained sample (US). Statistical analysis was performed using the Friedman test, with all comparisons made against untreated control. Differences were considered statistically significant at $*p < 0.05$, ** $p < 0.01$ or not significant (ns).

CD163 expression increased in the M1 control conditions (LPS and LPS + IFN-γ stimulation) and increased slightly in the M2 control condition (IL-10), although statistical significance was only reached for the first M1 control (LPS stimulation, **p<0.01) (***Figure 17C***).This observation is not in line with what is reported in the literature [168], as CD163 upregulation has been reported to be typically associated with M2a polarization (derived from IL-4 and IL-13 stimulation), rather than M2b and M2c profiles [169], However, several studies have shown that IL-10 can "prime" macrophages for M2a, M2b, or M2c polarization (without completely compromising them) [170] and can induce CD163 expression if macrophages are previously differentiated with M-CSF [148] as was done in this study (5.2.2 of Materials and Methods section). Therefore, an increase in expression of the M2 control (IL-10 stimulation) should have been observed, rather than the M1 controls (LPS stimulation and LPS + IFN-γ stimulation). Some aspects may account for this observation, as Purcu D. *et al*. reported that, although CD163 expression remains elevated at 72 hours, its peak expression is reached at 48 hours [148] and this time point should be considered in future studies. Furthermore, IL-10 has been shown to induce the production of Transforming Growth Factor Beta 1 (TGF-β1), which may also suppress CD163 expression to some extent [171]. Ultimately, the discrepancy in CD163 levels may also be attributed to donor variability, a condition inherent to experiments using primary human cells. Donor-derived macrophages can exhibit distinct basal activation states, receptor expression levels, and responsiveness to stimuli. All of these differences are influenced by genetic background, environmental exposures, and immune history, which may modulate the expression of surface markers such as CD163 [172]. Regarding cells stimulated with Chol-NP, there was no significant change in the expression of this marker compared to the control, indicating that Chol-NP do not modulate CD163 expression under the tested conditions.

CD206 expression was reduced under M1 control conditions and remained stable in cells treated with IL-10 (***Figure 17D***), as expected according to [173]. This pattern is consistent with the well-established association of CD206 with alternatively activated macrophages (M2 phenotypes), which are promoted by anti-inflammatory cytokines such as IL-10. In cells incubated with Chol-NP (***Figure 17D***), no statistically significant differences were observed in the expression of this marker, indicating that Chol-NP do not alter the regulatory mechanisms governing CD206 expression.

A decrease in the expression levels of the lineage marker CD14 was noted compared to the control in the scatter plots in ***Figures 17A*** and 17***B***. NP can interfere with signaling cascades, altering the recycling cycle of membrane receptors, as previously demonstrated, and thus inducing phenotypic shifts towards less mature activation states [174]. Previous studies indicate that CS can activate TLR4-mediated signaling pathways, in which CD14 acts as a co-receptor [175]. Furthermore, stimuli such as glucocorticoids [176], IL-13 [177] or LPS [178, 179] can inhibit its expression. It is plausible that NP induces similar changes, either by activating cellular stress pathways or promoting the release of anti-inflammatory mediators, contributing to a remodeling of the surface proteome, including a reduction in CD14.

The median fluorescence intensity (MFI) was also analyzed, providing a measure of the average amount of the marker expressed per cell, complementing the frequency data that indicates the percentage of cells positive for a given marker (***Figure 17E*** and 17***F***). A trend towards reduced CD206 expression (not statistically significant different) was observed in the presence of Chol-NP, as illustrated in ***Figure 17F***, but further assays with more donors would be required to confirm this trend.

Overall, from a biological safety perspective, the absence of upregulation of CD163 and CD206 suggests that Chol-NP are unlikely to trigger unintended activation of the signaling pathways associated with these markers.

3.2 Evaluation of the expression profile of CD86, CD40 and HLA-DR

The expression levels of CD86 (a costimulatory protein involved in T cell activation), CD40 (another costimulatory protein), and HLA-DR (a major histocompatibility complex class II protein, MHCII) were also evaluated to investigate a potential pro-inflammatory modulation induced by the NP (***Figure 18***). This hypothesis is supported by previous studies reporting that CS, used as the biopolymer for NP formulation, may promote an M1-like polarization profile [148].

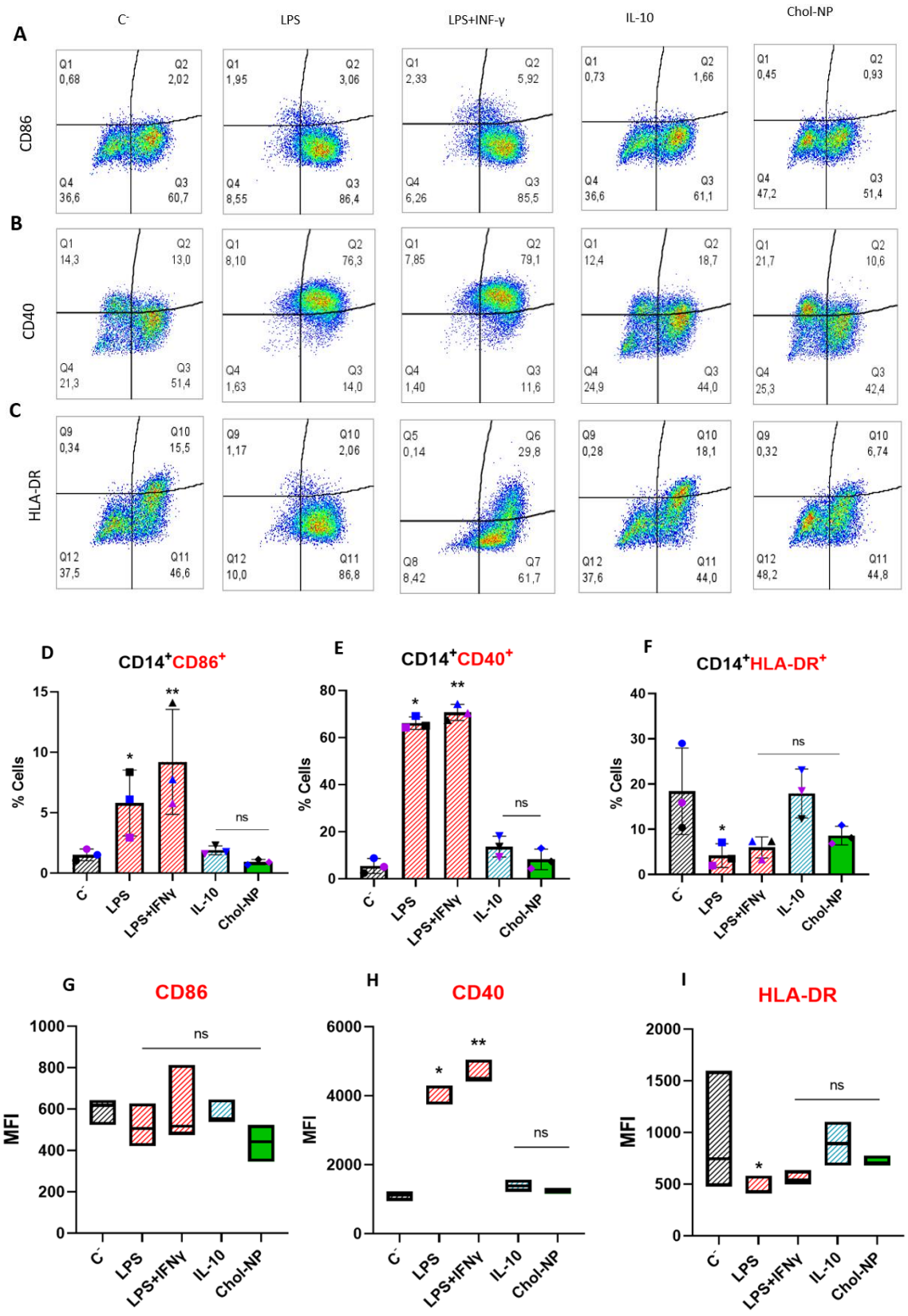


Figure 18. **Surface marker expression shown as scatter plots for A) CD86, B) CD40, and C) HLA-DR, and corresponding expression frequencies (% Cells) in D), E), and F), in human macrophages** (n = 3) differentiated in the presence of M-CSF for 7 days. Cells were then stimulated with Chol-NP, LPS (bacterial infection control, M1), LPS + IFN-γ (bacterial infection and inflammation control, M1), or IL-10 (anti-inflammatory control, M2) for 72 hours. "C–"

corresponds to the negative control (untreated cells). **Median fluorescence intensity (MFI) for G) CD86, H) CD40, and I) HLA-DR** was calculated by subtracting the fluorescence of the corresponding unstained sample (US). Statistical analysis was performed using the Friedman test, with all comparisons made against untreated control. Differences were considered statistically significant at $*p < 0.05$, ** $p < 0.01$ or not significant (ns).

CD86 was strongly expressed in M1 controls (LPS and LPS + IFN-γ) and downregulated in the M2 control (IL-10), consistent with previous studies [180, 181]. Furthermore, no significant differences in CD86 expression were observed in Chol-NP treated cells compared to the untreated control (***Figures 18D***). This suggests that Chol-NP does not promote proinflammatory M1 polarization under the conditions tested, indicating a lack of a stimulatory effect on macrophage activation via the CD86 pathway. Similarly, CD40 expression was elevated in M1 controls and reduced in the M2 control (***Figure 18E***) [182, 183]. Upon stimulation with Chol-NP, no significant changes in CD40 expression were observed, indicating that these NP do not induce costimulatory activation in macrophages via the CD40 pathway.

HLA-DR is a component of MHC class II typically associated with M1 polarization in response to pro-inflammatory stimuli, such as LPS [83]. However, the expression levels observed in the M1 controls did not reflect this pattern, which may be related to the time points used in the experiment (***Figure 18F***), as this molecule may be initially expressed and subsequently internalized [83]. Therefore, it would be relevant in future studies to assess HLA-DR expression at different stimulation times beyond the 72 hours used in this study, as described elsewhere [148]. Nevertheless, Chol-NP did not induce significant changes in HLA-DR expression under the settings used in these experiments (***Figure 18F***). MFI values were also analyzed and found to be consistent with the respective expression frequencies (***Figures 18G***, ***18H***, and ***18I***). Furthermore, there was a trend toward reduced MFI for CD86 in cells treated with Chol-NP.

According to the literature, the polarization capacity of CS depends on several factors, such as its purity, contaminants, and especially its degree of acetylation (DA) [78]. In the present study, CS was functionalized with norbornene groups (NorChit), with a substitution ratio of 0.38 group/CS monomer. Although the initial CS had a low DA (2-3%), typically associated with anti-inflammatory effects in human macrophages, the chemical modification with norbornene groups may have reduced the number of available amine groups. This could lead to a more pro-inflammatory macrophage response, as previously reported in studies using CS with a higher DA [184], than that used in this study.

Overall, the results, even though preliminary, indicate that Chol-NP did not induce significant changes in the expression of the surface markers analyzed and highlight the Chol-NP biocompatible profile to be used in a *H. pylori* infection scenario.

V. Conclusions and Future work

The main objective of this study was to establish the biological safety profile (cyto- and hemocompatibility profile, as well as the impact on macrophage polarization) of cholesterol-functionalized chitosan nanoparticles (Chol-NP), aimed to be used for *Helicobacter pylori* (*H. pylori*) gastric infection management. Establishing the NP biological safety profile is a crucial link on the chain for developing and validating a bioengineered therapeutic strategy.

Chol-NP did not significantly affect the metabolic activity of the gastric cell lines AGS (ATCC® CRL-1739) and MKN28 (ATCC® CRL-2947), and they also did not exhibit hemolytic profile, indicating that they are safe to be administered even to patients with active bleeding ulcers. As *H. pylori* infection is characterized by a highly inflammatory environment [87], the effect of Chol-NP on immune cells and its immunomodulatory potential were subsequently evaluated using human macrophages differentiated from monocytes isolated from the buffy coats of healthy donors. The results showed that Chol-NP did not impact macrophage metabolic activity. Furthermore, no modulatory effect on macrophage polarization was detected, and no significant changes in the expression levels of the analyzed surface markers (CD163, CD206, CD86, CD40 and HLA-DR) were reported to be associated with exposure to Chol-NP. Although Chol-NP did not promote macrophage transition to an anti-inflammatory phenotype, potentially beneficial for combating the inflammation associated to the *H. pylori* chronic infection, they also did not exacerbate inflammatory responses. Thus, the preliminary results herein depicted corroborate Chol-NP as cytocompatible and immune-safe within the context of *H. pylori* infection.

Future directions concerning the immuno-profile characterization of the Chol-NP include repeating experiments with a larger sample size and performing stimulation at multiple time points to better understand the dynamics of marker expression (e.g., HLA-DR and CD163), as well as analyzing the response for the NC-NP. It would also be interesting to analyze the macrophage culture supernatants via Enzyme-Linked Immunosorbent Assay (ELISA) to quantify the types and amounts of cytokines released, given that this secretory profile serves as a reliable indicator of macrophage polarization. Furthermore, given that Chol-NP did not induce polarization under basal conditions, it would be interesting to determine whether this remains true under pro-inflammatory conditions. To this end, a new experimental condition should be designed, in which macrophages would be stimulated with (lipopolysaccharide) LPS plus interferon-gamma (IFN-γ) and in the presence of Chol-NP. To complement the current findings, similar assays could be

extended to other immune cells, such as dendritic cells, which play a critical role in initiating adaptive immune responses, along with macrophages.

Another aspect to be addressed in the future involves the assessment of the possibility that NP may be internalized by macrophages. This could be monitored both spatially and temporally by labeling Chol-NP with fluorophores detectable by confocal microscopy.

Finally, additional omics-level analyses, including proteomic and genomic profiling, could be conducted to characterize the molecular landscape of NP-treated macrophages. Techniques such as mass spectrometry (MS), as well as DNA and RNA sequencing, could provide complementary insights into polarization profiles and elucidate cellular mechanisms related to lipid metabolism, apoptosis, phagocytosis, and other fundamental biological processes.

VI. References

1. Marshall, B. and J.R. Warren, *Unidentified curved bacilli in the stomach of patients with gastritis and peptic ulceration.* The lancet, 1984. **323**(8390): p. 1311-1315.
2. Marshall, B. and P.C. Adams, *Helicobacter pylori: A Nobel pursuit?* Canadian Journal of Gastroenterology, 2008. **22**(11): p. 895.
3. Fonseca, D.R., et al., *How to manage Helicobacter pylori infection beyond antibiotics: The bioengineering quest.* Applied Materials Today, 2024. **37**: p. 102123.
4. Krzyżek, P. and G. Gościniak, *Morphology of Helicobacter pylori as a result of peptidoglycan and cytoskeleton rearrangements.* Gastroenterology Review/Przegląd Gastroenterologiczny, 2018. **13**(3): p. 182-195.
5. Taylor, J.A., et al., *Localizing peptidoglycan synthesis in Helicobacter pylori using clickable metabolic probes.* Current protocols, 2021. **1**(4): p. e80.
6. Ierardi, E., et al., *The puzzle of coccoid forms of Helicobacter pylori: beyond basic science.* Antibiotics, 2020. **9**(6): p. 293.
7. Öztekin, M., et al., *Overview of Helicobacter pylori infection: clinical features, treatment, and nutritional aspects.* Diseases, 2021. **9**(4): p. 66.
8. Cheok, Y.Y., et al., *An overview of Helicobacter pylori survival tactics in the hostile human stomach environment.* Microorganisms, 2021. **9**(12): p. 2502.
9. Malfertheiner, P., et al., *Management of Helicobacter pylori infection: the Maastricht VI/Florence consensus report.* Gut, 2022.
10. Kumar, S., G.K. Patel, and U.C. Ghoshal, *Helicobacter pylori-induced inflammation: possible factors modulating the risk of gastric cancer.* Pathogens, 2021. **10**(9): p. 1099.
11. Lamb, A. and L.F. Chen, *Role of the Helicobacter pylori-Induced inflammatory response in the development of gastric cancer.* Journal of cellular biochemistry, 2013. **114**(3): p. 491-497.
12. Robinson, K., R.H. Argent, and J.C. Atherton, *The inflammatory and immune response to Helicobacter pylori infection.* Best practice & research Clinical gastroenterology, 2007. **21**(2): p. 237-259.
13. Baj, J., et al., *Mechanisms of the epithelial–mesenchymal transition and tumor microenvironment in Helicobacter pylori-induced gastric cancer.* Cells, 2020. **9**(4): p. 1055.

14. Peng, Z., et al., *Role of epithelial-mesenchymal transition in gastric cancer initiation and progression.* World J Gastroenterol, 2014. **20**(18): p. 5403-10.
15. Link, A., J. Bornschein, and C. Thon, *Helicobacter pylori induced gastric carcinogenesis-The best molecular model we have?* Best Practice & Research Clinical Gastroenterology, 2021. **50**: p. 101743.
16. Jaroenlapnopparat, A., K. Bhatia, and S. Coban, *Inflammation and gastric cancer.* Diseases, 2022. **10**(3): p. 35.
17. Salama, N.R., M.L. Hartung, and A. Müller, *Life in the human stomach: persistence strategies of the bacterial pathogen Helicobacter pylori.* Nat Rev Microbiol, 2013. **11**(6): p. 385-99.
18. Hsu, C.Y., et al., *Helicobacter pylori cholesterol-α-glucosyltransferase manipulates cholesterol for bacterial adherence to gastric epithelial cells.* Virulence, 2021. **12**(1): p. 2341-2351.
19. Lemos, F.F.B., et al., *Urea breath test for Helicobacter pylori infection in adult dyspeptic patients: A meta-analysis of diagnostic test accuracy.* World J Gastroenterol, 2024. **30**(6): p. 579-598.
20. Best, L.M., et al., *Non-invasive diagnostic tests for Helicobacter pylori infection.* Cochrane Database Syst Rev, 2018. **3**(3): p. Cd012080.
21. Kubo, K., et al., *Diagnostic Accuracy of a Novel Stool Antigen Test for Helicobacter pylori Infection in a Medical Checkup Setting: A Prospective Cohort Study.* Intern Med, 2024. **63**(11): p. 1525-1529.
22. Garcés-Durán, R., et al., *Endoscopic diagnosis of H. pylori infection.* Gastroenterol Hepatol, 2023. **46**(6): p. 483-488.
23. Malfertheiner, P., et al., *Helicobacter pylori infection.* Nat Rev Dis Primers, 2023. **9**(1): p. 19.
24. Ganz, R.A., et al., *Helicobacter pylori in patients can be killed by visible light.* Lasers Surg Med, 2005. **36**(4): p. 260-5.
25. Mamishi, S., et al., *Intrafamilial transmission of Helicobacter pylori: genotyping of faecal samples.* Br J Biomed Sci, 2016. **73**(1): p. 38-43.
26. Ibrahim, A., et al., *Sex-differences in the prevalence of Helicobacter pylori infection in pediatric and adult populations: Systematic review and meta-analysis of 244 studies.* Dig Liver Dis, 2017. **49**(7): p. 742-749.
27. Aumpan, N., V. Mahachai, and R.-k. Vilaichone, *Management of Helicobacter pylori infection.* JGH Open, 2023. **7**(1): p. 3-15.

28. Viegas, M.I., et al., *Effectiveness of First-Line Empirical Treatment in Portugal: Data from the European Registry on Helicobacter pylori Management.* GE - Portuguese Journal of Gastroenterology, 2024.
29. Molina-Castro, S., V. Ramírez-Mayorga, and W. Alpízar-Alpízar, *Priming the seed: Helicobacter pylori alters epithelial cell invasiveness in early gastric carcinogenesis.* World Journal of Gastrointestinal Oncology, 2018. **10**(9): p. 231.
30. Costa, K., et al., *The morphological transition of Helicobacter pylori cells from spiral to coccoid is preceded by a substantial modification of the cell wall.* Journal of Bacteriology, 1999. **181**(12): p. 3710-3715.
31. Dunne, C., B. Dolan, and M. Clyne, *Factors that mediate colonization of the human stomach by Helicobacter pylori.* World Journal of Gastroenterology: WJG, 2014. **20**(19): p. 5610.
32. Debowski, A.W., et al., *Helicobacter pylori gene silencing in vivo demonstrates urease is essential for chronic infection.* PLoS pathogens, 2017. **13**(6): p. e1006464.
33. Krzyżek, P., V. Puca, and R. Grande, *Helicobacter pylori and its mechanisms of antibiotic survival.* Frontiers in Cellular and Infection Microbiology, 2023. **13**: p. 1164227.
34. Enroth, H., et al., *In vitro aging of Helicobacter pylori: changes in morphology, intracellular composition and surface properties.* Helicobacter, 1999. **4**(1): p. 7-16.
35. Maia, A.M.F., *Epidemiologia, patogénese e diagnóstico microbiológico de Helicobacter pylori*. 2020, Universidade do Porto (Portugal).
36. Cover, T.L. and S.R. Blanke, *Helicobacter pylori VacA, a paradigm for toxin multifunctionality.* Nature Reviews Microbiology, 2005. **3**(4): p. 320-332.
37. Chaturvedi, R., et al., *Activation of EGFR and ERBB2 by Helicobacter pylori results in survival of gastric epithelial cells with DNA damage.* Gastroenterology, 2014. **146**(7): p. 1739-1751. e14.
38. Tegtmeyer, N., et al., *Unique TLR9 activation by Helicobacter pylori depends on the cag T4SS, but not on VirD2 relaxases or VirD4 coupling proteins.* Current Microbiology, 2022. **79**(4): p. 121.
39. Li, S., et al., *How long will it take to launch an effective Helicobacter pylori vaccine for humans?* Infection and drug resistance, 2023: p. 3787-3805.
40. Foegeding, N.J., et al., *An overview of Helicobacter pylori VacA toxin biology.* Toxins, 2016. **8**(6): p. 173.

41. Palframan, S.L., T. Kwok, and K. Gabriel, *Vacuolating cytotoxin A (VacA), a key toxin for Helicobacter pylori pathogenesis.* Frontiers in cellular and infection microbiology, 2012. **2**: p. 92.
42. Hisatsune, J., et al., *Helicobacter pylori VacA enhances prostaglandin E2 production through induction of cyclooxygenase 2 expression via a p38 mitogen-activated protein kinase/activating transcription factor 2 cascade in AZ-521 cells.* Infect Immun, 2007. **75**(9): p. 4472-81.
43. Jarzab, M., et al., *Helicobacter pylori-derived outer membrane vesicles (OMVs): role in bacterial pathogenesis?* Microorganisms, 2020. **8**(9): p. 1328.
44. Hathroubi, S., et al., *Helicobacter pylori biofilm formation and its potential role in pathogenesis.* Microbiology and Molecular Biology Reviews, 2018. **82**(2): p. 10.1128/mmbr. 00001-18.
45. Appelmelk, B.J. and C.M. Vandenbroucke-Grauls, *Lipopolysaccharide Lewis Antigens.* Helicobacter pylori: physiology and genetics, 2001: p. 419-428.
46. Fan, J., J. Zhu, and H. Xu, *Strategies of Helicobacter pylori in evading host innate and adaptive immunity: insights and prospects for therapeutic targeting.* Frontiers in Cellular and Infection Microbiology, 2024. **14**: p. 1342913.
47. Pachathundikandi, S.K., et al., *Interplay of the Gastric Pathogen Helicobacter pylori with Toll-Like Receptors.* Biomed Res Int, 2015. **2015**: p. 192420.
48. Sirit, I.S. and R.M. Peek, Jr., *Decoding the Ability of Helicobacter pylori to Evade Immune Recognition and Cause Disease.* Cell Mol Gastroenterol Hepatol, 2025. **19**(5): p. 101470.
49. Karkhah, A., et al., *Helicobacter pylori evasion strategies of the host innate and adaptive immune responses to survive and develop gastrointestinal diseases.* Microbiol Res, 2019. **218**: p. 49-57.
50. Lavelle, E.C., et al., *The role of TLRs, NLRs, and RLRs in mucosal innate immunity and homeostasis.* Mucosal Immunol, 2010. **3**(1): p. 17-28.
51. Sijmons, D., et al., *Helicobacter pylori and the Role of Lipopolysaccharide Variation in Innate Immune Evasion.* Front Immunol, 2022. **13**: p. 868225.
52. Blaser, M.J. and J.C. Atherton, *Helicobacter pylori persistence: biology and disease.* J Clin Invest, 2004. **113**(3): p. 321-33.
53. Matsuura, M., *Structural Modifications of Bacterial Lipopolysaccharide that Facilitate Gram-Negative Bacteria Evasion of Host Innate Immunity.* Front Immunol, 2013. **4**: p. 109.

54. Kim, J.H., et al., *Helicobacter pylori flagellin: TLR5 evasion and fusion-based conversion into a TLR5 agonist.* Biochem Biophys Res Commun, 2018. **505**(3): p. 872-878.
55. Varga, M.G., et al., *TLR9 activation suppresses inflammation in response to Helicobacter pylori infection.* Am J Physiol Gastrointest Liver Physiol, 2016. **311**(5): p. G852-g858.
56. Dooyema, S.D.R., et al., *Helicobacter pylori actively suppresses innate immune nucleic acid receptors.* Gut Microbes, 2022. **14**(1): p. 2105102.
57. Wang, G., et al., *Peptidoglycan deacetylation in Helicobacter pylori contributes to bacterial survival by mitigating host immune responses.* Infect Immun, 2010. **78**(11): p. 4660-6.
58. Brancewicz, J., et al., *The Multifaceted Role of Macrophages in Biology and Diseases.* Int J Mol Sci, 2025. **26**(5).
59. Ayala, G., et al., *Exploring alternative treatments for Helicobacter pylori infection.* World J Gastroenterol, 2014. **20**(6): p. 1450-69.
60. D'Elios, M.M., et al., *Helicobacter pylori, T cells and cytokines: the "dangerous liaisons".* FEMS Immunology & Medical Microbiology, 2005. **44**(2): p. 113-119.
61. Kabir, S., *The role of interleukin-17 in the Helicobacter pylori induced infection and immunity.* Helicobacter, 2011. **16**(1): p. 1-8.
62. Raghavan, S. and M. Quiding-Järbrink, *Immune modulation by regulatory T cells in Helicobacter pylori-associated diseases.* Endocr Metab Immune Disord Drug Targets, 2012. **12**(1): p. 71-85.
63. Zhang, H., et al., *Helicobacter pylori Colonization Protects Against Chronic Experimental Colitis by Regulating Th17/Treg Balance.* Inflamm Bowel Dis, 2018. **24**(7): p. 1481-1492.
64. Mohammadi, M., et al., *Helicobacter-specific cell-mediated immune responses display a predominant Th1 phenotype and promote a delayed-type hypersensitivity response in the stomachs of mice.* J Immunol, 1996. **156**(12): p. 4729-38.
65. *Cholesterol: a bacterial scarlet letter?* Lab Animal, 2006. **35**(10): p. 8-8.
66. McGee, D.J., et al., *Cholesterol enhances Helicobacter pylori resistance to antibiotics and LL-37.* Antimicrob Agents Chemother, 2011. **55**(6): p. 2897-904.
67. Hutton, M.L., et al., *A Helicobacter pylori Homolog of Eukaryotic Flotillin Is Involved in Cholesterol Accumulation, Epithelial Cell Responses and Host Colonization.* Front Cell Infect Microbiol, 2017. **7**: p. 219.

68. Ito, Y., et al., *Helicobacter pylori cholesteryl α-glucosides contribute to its pathogenicity and immune response by natural killer T cells.* PLoS One, 2013. **8**(12): p. e78191.
69. Kinjo, Y. and K. Ueno, *iNKT cells in microbial immunity: recognition of microbial glycolipids.* Microbiology and Immunology, 2011. **55**(7): p. 472-482.
70. Jan, H.M., et al., *Cholesteryl α-D-glucoside 6-acyltransferase enhances the adhesion of Helicobacter pylori to gastric epithelium.* Commun Biol, 2020. **3**(1): p. 120.
71. Morey, P., et al., *Helicobacter pylori Depletes Cholesterol in Gastric Glands to Prevent Interferon Gamma Signaling and Escape the Inflammatory Response.* Gastroenterology, 2018. **154**(5): p. 1391-1404.e9.
72. Seif, F., et al., *The role of JAK-STAT signaling pathway and its regulators in the fate of T helper cells.* Cell Commun Signal, 2017. **15**(1): p. 23.
73. Wiesner, J. and A. Vilcinskas, *Antimicrobial peptides: the ancient arm of the human immune system.* Virulence, 2010. **1**(5): p. 440-64.
74. Pinho, A.S., et al., *Cholesterol Functionalized Nanoparticles Are Effective against Helicobacter pylori, the Gastric Bug: A Proof-of-Concept Study.* Adv Healthc Mater, 2025. **14**(10): p. e2404065.
75. Fei, X., et al., *Macrophage biology in the pathogenesis of Helicobacter pylori infection.* Crit Rev Microbiol, 2025. **51**(3): p. 399-416.
76. Malech, H.L., F.R. Deleo, and M.T. Quinn, *The role of neutrophils in the immune system: an overview.* Methods Mol Biol, 2014. **1124**: p. 3-10.
77. Patel, A.A., et al., *The fate and lifespan of human monocyte subsets in steady state and systemic inflammation.* J Exp Med, 2017. **214**(7): p. 1913-1923.
78. Oliveira, M., et al., *Chitosan drives anti-inflammatory macrophage polarisation and pro-inflammatory dendritic cell stimulation.* European cells & materials, 2012. **24**: p. 136-52; discussion 152.
79. Chaintreuil, P., et al., *The generation, activation, and polarization of monocyte-derived macrophages in human malignancies.* Front Immunol, 2023. **14**: p. 1178337.
80. Yao, Y., X.H. Xu, and L. Jin, *Macrophage Polarization in Physiological and Pathological Pregnancy.* Front Immunol, 2019. **10**: p. 792.
81. Yang, H., et al., *The Role of Adhesion in Helicobacter pylori Persistent Colonization.* Curr Microbiol, 2023. **80**(5): p. 185.
82. Benoit, M., B. Desnues, and J.L. Mege, *Macrophage polarization in bacterial infections.* J Immunol, 2008. **181**(6): p. 3733-9.

83. Unuvar Purcu, D., et al., *Effect of stimulation time on the expression of human macrophage polarization markers.* PLoS One, 2022. **17**(3): p. e0265196.
84. Tan, G.M.Y., et al., *Suppression of cell division-associated genes by Helicobacter pylori attenuates proliferation of RAW264.7 monocytic macrophage cells.* Scientific Reports, 2015. **5**(1): p. 11046.
85. Strizova, Z., et al., *M1/M2 macrophages and their overlaps - myth or reality?* Clin Sci (Lond), 2023. **137**(15): p. 1067-1093.
86. Luo, M., et al., *Macrophage polarization: an important role in inflammatory diseases.* Front Immunol, 2024. **15**: p. 1352946.
87. Wang, X., et al., *Helicobacter pylori triggers inflammation and oncogenic transformation by perturbing the immune microenvironment.* Biochim Biophys Acta Rev Cancer, 2024. **1879**(5): p. 189139.
88. Wang, Y., et al., *Macrophage-derived extracellular vesicles: diverse mediators of pathology and therapeutics in multiple diseases.* Cell Death Dis, 2020. **11**(10): p. 924.
89. Zhang, Q. and M. Sioud, *Tumor-Associated Macrophage Subsets: Shaping Polarization and Targeting.* Int J Mol Sci, 2023. **24**(8).
90. Fei, X., et al., *Helicobacter pylori infection promotes M1 macrophage polarization and gastric inflammation by activation of NLRP3 inflammasome via TNF/TNFR1 axis.* Cell Commun Signal, 2025. **23**(1): p. 6.
91. Wei, Y.F., et al., *Helicobacter pylori disrupts gastric mucosal homeostasis by stimulating macrophages to secrete CCL3.* Cell Commun Signal, 2024. **22**(1): p. 263.
92. Belenichev, I., et al., *Modulating Nitric Oxide: Implications for Cytotoxicity and Cytoprotection.* Antioxidants (Basel), 2024. **13**(5).
93. Quiding-Järbrink, M., S. Raghavan, and M. Sundquist, *Enhanced M1 macrophage polarization in human helicobacter pylori-associated atrophic gastritis and in vaccinated mice.* PLoS One, 2010. **5**(11): p. e15018.
94. Duan, Y., et al., *Helicobacter pylori and gastric cancer: mechanisms and new perspectives.* J Hematol Oncol, 2025. **18**(1): p. 10.
95. den Hartog, G., et al., *Regulation of Rac1 and Reactive Oxygen Species Production in Response to Infection of Gastrointestinal Epithelia.* PLoS Pathog, 2016. **12**(1): p. e1005382.
96. Roberts, L.T., et al., *Helicobacter Pylori: A Review of Current Treatment Options in Clinical Practice.* Life (Basel), 2022. **12**(12).

97. Shiotani, A., et al., *Treating Helicobacter pylori effectively while minimizing misuse of antibiotics.* Cleve Clin J Med, 2017. **84**(4): p. 310-318.
98. Shiotani, A., et al., *Helicobacter pylori diagnosis and therapy in the era of antimicrobial stewardship.* Therap Adv Gastroenterol, 2021. **14**: p. 17562848211064080.
99. Suzuki, S., et al., *The Ideal Helicobacter pylori Treatment for the Present and the Future.* Digestion, 2022. **103**(1): p. 62-68.
100. Graham, D.Y., et al., *Twice a day quadruple therapy (bismuth subsalicylate, tetracycline, metronidazole plus lansoprazole) for treatment of Helicobacter pylori infection.* Aliment Pharmacol Ther, 1997. **11**(5): p. 935-8.
101. Mladenova, I., *Clinical Relevance of Helicobacter pylori Infection.* J Clin Med, 2021. **10**(16).
102. Sun, L., et al., *Antibiotic-Induced Disruption of Gut Microbiota Alters Local Metabolomes and Immune Responses.* Front Cell Infect Microbiol, 2019. **9**: p. 99.
103. Yunle, K., et al., *Advances in Helicobacter pylori vaccine research: From candidate antigens to adjuvants-A review.* Helicobacter, 2024. **29**(1): p. e13034.
104. Ji, J. and H. Yang, *Using Probiotics as Supplementation for Helicobacter pylori Antibiotic Therapy.* Int J Mol Sci, 2020. **21**(3).
105. Baryshnikova, N.V., et al., *Probiotics and autoprobiotics for treatment of Helicobacter pylori infection.* World J Clin Cases, 2023. **11**(20): p. 4740-4751.
106. Sathianarayanan, S., et al., *A new approach against Helicobacter pylori using plants and its constituents: A review study.* Microb Pathog, 2022. **168**: p. 105594.
107. Al-Rooqi, M.M., et al., *Flavonoids and related privileged scaffolds as potential urease inhibitors: a review.* RSC Adv, 2023. **13**(5): p. 3210-3233.
108. Cardos, I.A., et al., *Revisiting Therapeutic Strategies for H. pylori Treatment in the Context of Antibiotic Resistance: Focus on Alternative and Complementary Therapies.* Molecules, 2021. **26**(19).
109. Mandici, A., A.-A. Covrig, and I. Macovei, *Food phytochemicals against Helicobacter pylori.* Romanian Journal of Pharmaceutical Practice, 2021. **14**: p. 11-17.
110. Elbehiry, A., et al., *Helicobacter pylori: Routes of Infection, Antimicrobial Resistance, and Alternative Therapies as a Means to Develop Infection Control.* Diseases, 2024. **12**(12).
111. Imoto, I., et al., *Antimicrobial Effects of Lactoferrin against Helicobacter pylori Infection.* Pathogens, 2023. **12**(4).

112. Chitas, R., et al., *Targeted nanotherapeutics for the treatment of Helicobacter pylori infection.* J Biomed Sci, 2024. **31**(1): p. 78.
113. Muñoz, A.B., et al., *Bacteriophages of Helicobacter pylori.* Front Microbiol, 2020. **11**: p. 549084.
114. Khan, I., K. Saeed, and I. Khan, *Nanoparticles: Properties, applications and toxicities.* Arabian Journal of Chemistry, 2019. **12**(7): p. 908-931.
115. TM, M.W., W.M. Lau, and V.V. Khutoryanskiy, *Chitosan and Its Derivatives for Application in Mucoadhesive Drug Delivery Systems.* Polymers (Basel), 2018. **10**(3).
116. Gonçalves, I.C., et al., *The potential utility of chitosan micro/nanoparticles in the treatment of gastric infection.* Expert Rev Anti Infect Ther, 2014. **12**(8): p. 981-92.
117. Luo, M., et al., *Construction and optimization of pH-sensitive nanoparticle delivery system containing PLGA and UCCs-2 for targeted treatment of Helicobacter pylori.* Colloids Surf B Biointerfaces, 2018. **164**: p. 11-19.
118. Arangoa, M.A., et al., *Bioadhesive potential of gliadin nanoparticulate systems.* Eur J Pharm Sci, 2000. **11**(4): p. 333-41.
119. Xu, Y., et al., *Surface Modification of Lipid-Based Nanoparticles.* ACS Nano, 2022. **16**(5): p. 7168-7196.
120. Yuan, X., et al., *Target challenging-cancer drug delivery to gastric cancer tissues with a fucose graft epigallocatechin-3-gallate-gold particles nanocomposite approach.* J Photochem Photobiol B, 2018. **183**: p. 147-153.
121. Ouellette, M., et al., *Insights into gold nanoparticles as a mucoadhesive system.* Scientific Reports, 2018. **8**(1): p. 14357.
122. Bose, A., et al., *Nanomicelles: Types, properties and applications in drug delivery.* IET Nanobiotechnol, 2021. **15**(1): p. 19-27.
123. Omanovic-Miklicanin, E., et al., *Nanocomposites: a brief review.* Health and Technology, 2019. **10**: p. 51 - 59.
124. Gonçalves, I.C., et al., *Bacteria-targeted biomaterials: Glycan-coated microspheres to bind Helicobacter pylori.* Acta Biomater, 2016. **33**: p. 40-50.
125. Jing, Z.W., et al., *Design and evaluation of novel pH-sensitive ureido-conjugated chitosan/TPP nanoparticles targeted to Helicobacter pylori.* Biomaterials, 2016. **84**: p. 276-285.
126. Luo, Q., et al., *Research progress in photodynamic therapy for Helicobacter pylori infection.* Helicobacter, 2024. **29**(2): p. e13068.

127. Meng, F., et al., *Nanocluster-mediated photothermia improves eradication efficiency and antibiotic sensitivity of Helicobacter pylori.* Cancer Nanotechnology, 2022. **13**(1): p. 13.
128. Liu, T., et al., *A nanoparticle-based sonodynamic therapy reduces Helicobacter pylori infection in mouse without disrupting gut microbiota.* Nat Commun, 2024. **15**(1): p. 844.
129. Collado-González, M. and M. Esteban, *Chitosan-nanoparticles effects on mucosal immunity: A systematic review.* Fish Shellfish Immunol, 2022. **130**: p. 1-8.
130. Abourehab, M.A.S., et al., *Recent Advances of Chitosan Formulations in Biomedical Applications.* Int J Mol Sci, 2022. **23**(18).
131. Ben Amor, I., et al., *Chitosan: A Green Approach to Metallic Nanoparticle/Nanocomposite Synthesis and Applications.* Polymers (Basel), 2024. **16**(18).
132. Gierszewska, M. and J. Ostrowska-Czubenko, *Chitosan-based membranes with different ionic crosslinking density for pharmaceutical and industrial applications.* Carbohydr Polym, 2016. **153**: p. 501-511.
133. Sogias, I.A., A.C. Williams, and V.V. Khutoryanskiy, *Why is chitosan mucoadhesive?* Biomacromolecules, 2008. **9**(7): p. 1837-42.
134. Guarnieri, A., et al., *Antimicrobial properties of chitosan from different developmental stages of the bioconverter insect Hermetia illucens.* Sci Rep, 2022. **12**(1): p. 8084.
135. Fonseca, D.R., et al., *One-Pot Microfluidics to Engineer Chitosan Nanoparticles Conjugated with Antimicrobial Peptides Using "Photoclick" Chemistry: Validation Using the Gastric Bacterium Helicobacter pylori.* ACS Applied Materials & Interfaces, 2024. **16**(12): p. 14533-14547.
136. Moosazadeh Moghaddam, M., et al., *Targeted delivery of a short antimicrobial peptide (CM11) against Helicobacter pylori gastric infection using concanavalin A-coated chitosan nanoparticles.* J Mater Sci Mater Med, 2023. **34**(9): p. 44.
137. Spósito, L., et al., *Engineering resveratrol-loaded chitosan nanoparticles for potential use against Helicobacter pylori infection.* Eur J Pharm Biopharm, 2024. **199**: p. 114280.
138. Jha, R. and R.A. Mayanovic, *A Review of the Preparation, Characterization, and Applications of Chitosan Nanoparticles in Nanomedicine.* Nanomaterials (Basel), 2023. **13**(8).

139. Wang, Z., F. Yu, and F. Hu, *Functional Chitosan and Its Derivative-Related Drug Delivery Systems for Nano-Therapy: Recent Advances.* Pharmaceutics, 2024. **16**(3).
140. Alves, P., et al., *Thiol–Norbornene Photoclick Chemistry for Grafting Antimicrobial Peptides onto Chitosan to Create Antibacterial Biomaterials.* ACS Applied Polymer Materials, 2022. **4**.
141. Alves, P., et al., *Norbornene-chitosan spray-dried microspheres for peptide conjugation using thiol-ene "photoclick" chemistry Premio Áccesit Congreso SIBB 2022 8.* Biomecánica, 2022. **30**: p. 7-15.
142. Kumari, S., et al., *A comprehensive review on various techniques used for synthesizing nanoparticles.* Journal of Materials Research and Technology, 2023. **27**: p. 1739-1763.
143. Gimondi, S., et al., *Microfluidic Devices: A Tool for Nanoparticle Synthesis and Performance Evaluation.* ACS Nano, 2023. **17**(15): p. 14205-14228.
144. Schwalm, R., *Photoinitiators and Photopolymerization*, in *Encyclopedia of Materials: Science and Technology*, K.H.J. Buschow, et al., Editors. 2001, Elsevier: Oxford. p. 6946-6951.
145. Holmes, R., et al., *Thiol-Ene Photo-Click Collagen-PEG Hydrogels: Impact of Water-Soluble Photoinitiators on Cell Viability, Gelation Kinetics and Rheological Properties.* Polymers (Basel), 2017. **9**(6).
146. Fisher, S.A., A.E.G. Baker, and M.S. Shoichet, *Designing Peptide and Protein Modified Hydrogels: Selecting the Optimal Conjugation Strategy.* J Am Chem Soc, 2017. **139**(22): p. 7416-7427.
147. Pinto, A.M., et al., *Smaller particle size and higher oxidation improves biocompatibility of graphene-based materials.* Carbon, 2016. **99**: p. 318-329.
148. Castro, F., et al., *Pro-inflammatory chitosan/poly(γ-glutamic acid) nanoparticles modulate human antigen-presenting cells phenotype and revert their pro-invasive capacity.* Acta Biomaterialia, 2017. **63**: p. 96-109.
149. Jesus, S., et al., *Chitosan Nanoparticles: Shedding Light on Immunotoxicity and Hemocompatibility.* Front Bioeng Biotechnol, 2020. **8**: p. 100.
150. Sánchez-Iglesias, A., et al., *Hydrophobic Interactions Modulate Self-Assembly of Nanoparticles.* ACS Nano, 2012. **6**(12): p. 11059-11065.
151. A. Sofia Pinho, D.S., Victoria Leiro, Mette Klitgaard, Anette Müllertz, M. Cristina L. Martins and Paula Parreira, *Sterol-grafted chitosan nanoparticles as bactericidal nano-decoys against Helicobacter pylori*. 2025 (in preparation).

152. Guo, C., et al., *Natural products for gastric carcinoma prevention and treatment: Focus on their antioxidant stress actions in the Correa's cascade.* Phytomedicine, 2024. **123**: p. 155253.
153. Backert, S., et al., *Gene expression and protein profiling of AGS gastric epithelial cells upon infection with Helicobacter pylori.* Proteomics, 2005. **5**(15): p. 3902-18.
154. Yokozaki, H., *Molecular characteristics of eight gastric cancer cell lines established in Japan.* Pathol Int, 2000. **50**(10): p. 767-77.
155. Henriques, P.C., et al., *Orally administrated chitosan microspheres bind Helicobacter pylori and decrease gastric infection in mice.* Acta Biomater, 2020. **114**: p. 206-220.
156. Lopes-de-Campos, D., et al., *Targeting and killing the Ever-Challenging ulcer bug.* Int J Pharm, 2022. **617**: p. 121582.
157. Fan, Z., et al., *Cytotoxic effects of NIR responsive chitosan-polymersome layer coated melatonin-upconversion nanoparticles on HGC27 and AGS gastric cancer cells: Role of the ROS/PI3K/Akt/mTOR signaling pathway.* Int J Biol Macromol, 2024. **278**(Pt 1): p. 134187.
158. Luo, H., et al., *N-Succinyl-chitosan nanoparticles induced mitochondria-dependent apoptosis in K562.* Mol Cell Probes, 2012. **26**(4): p. 164-9.
159. Popa, D.G., et al., *Role of Helicobacter pylori in the triggering and evolution of hemorrhagic gastro-duodenal lesions.* Exp Ther Med, 2021. **22**(4): p. 1147.
160. Urbán, P., N.J. Liptrott, and S. Bremer, *Overview of the blood compatibility of nanomedicines: A trend analysis of in vitro and in vivo studies.* Wiley Interdiscip Rev Nanomed Nanobiotechnol, 2019. **11**(3): p. e1546.
161. Mylvaganam, S., S.A. Freeman, and S. Grinstein, *The cytoskeleton in phagocytosis and macropinocytosis.* Current Biology, 2021. **31**(10): p. R619-R632.
162. Cardoso, A.P., et al., *Matrix metalloproteases as maestros for the dual role of LPS- and IL-10-stimulated macrophages in cancer cell behaviour.* BMC Cancer, 2015. **15**(1): p. 456.
163. Londono, R., et al., *The effect of cell debris within biologic scaffolds upon the macrophage response.* J Biomed Mater Res A, 2017. **105**(8): p. 2109-2118.
164. Zhao, X., et al., *Negatively charged phospholipids accelerate the membrane fusion activity of the plant-specific insert domain of an aspartic protease.* J Biol Chem, 2022. **298**(1): p. 101430.

165. Xia, T., et al., *Advances in the study of macrophage polarization in inflammatory immune skin diseases.* Journal of Inflammation, 2023. **20**(1): p. 33.
166. Barker, R.N., et al., *Antigen presentation by macrophages is enhanced by the uptake of necrotic, but not apoptotic, cells.* Clin Exp Immunol, 2002. **127**(2): p. 220-5.
167. Ambarus, C.A., et al., *Systematic validation of specific phenotypic markers for in vitro polarized human macrophages.* J Immunol Methods, 2012. **375**(1-2): p. 196-206.
168. Porcheray, F., et al., *Macrophage activation switching: an asset for the resolution of inflammation.* Clin Exp Immunol, 2005. **142**(3): p. 481-9.
169. Mantovani, A., et al., *The chemokine system in diverse forms of macrophage activation and polarization.* Trends Immunol, 2004. **25**(12): p. 677-86.
170. Hamilton, T.A., et al., *Myeloid Colony-Stimulating Factors as Regulators of Macrophage Polarization.* Frontiers in Immunology, 2014. **Volume 5 - 2014**.
171. Pioli, P.A., et al., *TGF-beta regulation of human macrophage scavenger receptor CD163 is Smad3-dependent.* J Leukoc Biol, 2004. **76**(2): p. 500-8.
172. Taciak, B., et al., *Unveiling the Phenotypic Variability of Macrophages: Insights from Donor Diversity and Pooling Strategies.* Int J Mol Sci, 2025. **26**(3).
173. Xu, Z.J., et al., *The M2 macrophage marker CD206: a novel prognostic indicator for acute myeloid leukemia.* Oncoimmunology, 2020. **9**(1): p. 1683347.
174. de Almeida, M.S., et al., *Understanding nanoparticle endocytosis to improve targeting strategies in nanomedicine.* Chemical society reviews, 2021. **50**(9): p. 5397-5434.
175. Zhang, P., et al., *Toll like receptor 4 (TLR4) mediates the stimulating activities of chitosan oligosaccharide on macrophages.* Int Immunopharmacol, 2014. **23**(1): p. 254-61.
176. Ivy, R.K., et al., *Down regulation of CD14 expression through pretreatment with glucocorticoids.* Biomed Sci Instrum, 2003. **39**: p. 506-10.
177. Cosentino, G., et al., *IL-13 down-regulates CD14 expression and TNF-alpha secretion in normal human monocytes.* J Immunol, 1995. **155**(6): p. 3145-51.
178. Lin, S.M., et al., *Differential regulation of membrane CD14 expression and endotoxin-tolerance in alveolar macrophages.* Am J Respir Cell Mol Biol, 2004. **31**(2): p. 162-70.
179. Dobrovolskaia, M.A. and S.N. Vogel, *Toll receptors, CD14, and macrophage activation and deactivation by LPS.* Microbes and Infection, 2002. **4**(9): p. 903-914.

180. Smith, T.D., et al., *Regulation of macrophage polarization and plasticity by complex activation signals.* Integr Biol (Camb), 2016. **8**(9): p. 946-55.
181. Mittal, S.K., et al., *Interleukin 10 (IL-10)-mediated Immunosuppression: MARCH-I INDUCTION REGULATES ANTIGEN PRESENTATION BY MACROPHAGES BUT NOT DENDRITIC CELLS.* J Biol Chem, 2015. **290**(45): p. 27158-27167.
182. Qin, H., et al., *LPS induces CD40 gene expression through the activation of NF-kappaB and STAT-1alpha in macrophages and microglia.* Blood, 2005. **106**(9): p. 3114-22.
183. Qin, H., et al., *IL-10 inhibits lipopolysaccharide-induced CD40 gene expression through induction of suppressor of cytokine signaling-3.* J Immunol, 2006. **177**(11): p. 7761-71.
184. Barbosa, J.N., et al., *Evaluation of the effect of the degree of acetylation on the inflammatory response to 3D porous chitosan scaffolds.* J Biomed Mater Res A, 2010. **93**(1): p. 20-8.